

AD-A688 413

AIR FORCE INST OF TECH WRIGHT-PATTERSON AFB OH 45900--ETC F/8 89/12
SLOW DISCHARGE OPTICAL SPECTROSCOPY OF ION IMPLANTED GALLIUM AR--ETC(U)
DEC 79 S PANGSTMAN
AFIT/GE/EE/T90-89

UNCLASSIFIED

AL

12
AD-A688 413



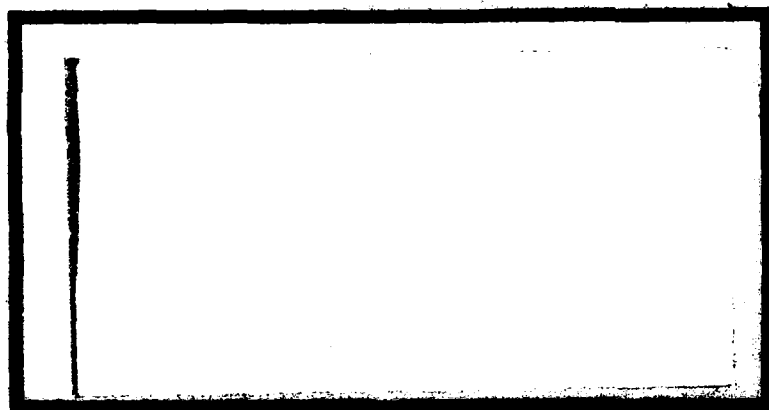
END
DATA
FILMED
3 - 80
BDC



Q

LEVEL

DDC
RECEIVED
FEB 7 1980
A



UNITED STATES AIR FORCE
AIR UNIVERSITY
AIR FORCE INSTITUTE OF TECHNOLOGY
Wright-Patterson Air Force Base, Ohio

6 GLOW DISCHARGE OPTICAL SPECTROSCOPY
OF ION IMPLANTED GALLIUM ARSENIDE

9 Master's THESIS,

14 AFIT/GE/EE/79D-29

10 Suk Puangthum
2Lt RTAF

11 Dec 79

12 86
1

DDC
RECEIVED
3 2 1980

Approved for public release; distribution unlimited.

012 755

mit

AFIT/GE/EE/79D-29

GLOW DISCHARGE OPTICAL SPECTROSCOPY
OF ION IMPLANTED GALLIUM ARSENIDE

THESIS

Presented to the Faculty of the School of Engineering
of the Air Force Institute of Technology
Air Training Command
in Partial Fulfillment of the
Requirements for the Degree of
Master of Science

by

Suk Puangthum, B.S.E.E.

2nd Lt.

RTAF

Graduate Electrical Engineering

December 1979

Approved for public release; distribution unlimited.

Preface

This thesis addresses a subject which is both a matter of practical importance in semiconductor technology and an excellent opportunity for a learning experience. One important goal of the original research program, to improve the sensitivity of the Glow Discharge Optical Spectroscopy (GDOS) apparatus, was not achieved due to time constraints and the risk that lengthy down time of the apparatus would interfere with the primary task. The initial plan to study both Si and Mg implants was modified when no meaningful Si data could be obtained. After much time and effort, the problem was found to lie in the implantation process itself. As a result, only Mg implants are analyzed in this thesis.

I would like to thank Dr. Y.S. Park and 1Lt Bill Theis, my laboratory research advisor. I would like to thank also other laboratory personnel including Jim Ehret, Charlie Geesner and Rick Patton, all of whom were very helpful. I am very much indebted to Dr. Seung Yun of Ohio University for teaching me on GDOS and his calibration of magnesium impurity.

My very special thanks go to Capt. M. Borky who is my thesis and Electronic Device Technology sequence advisor. His advice was helpful. His friendliness and willingness to help was the big factor in finishing this thesis. I consider myself to be very fortunate to have had him as one of my teachers.

Contents

	<u>Page</u>
Preface	ii
List of Figures	v
List of Tables	vi
Abstract	vii
I. Introduction	1
Background	1
Objectives	3
Scope	3
Results	4
Organization of Report	5
II. Ion Implantation	6
History	6
The Process	7
Energy Loss Equations	7
Ion Range Distribution	13
Channelling in Single Crystal Materials	16
Radiation Damage and Annealing	17
III. Glow Discharges	19
Glow Discharges	19
Sputtering	21
IV. Glow Discharge Optical Spectroscopy (GDOS)	23
Principle	23
Determination of Impurity Concentration	24
Sputtering Rate Determination	26
GDOS System Calibration	26
V. Experimental Apparatus	34
Sputtering Chamber Assembly	34
Vacuum, Gas, and Cooling System	38
Detecting and Recording Systems	39

	<u>Page</u>
VI. Illumination of the Entrance Slit.	42
Principle of Slit Illumination	42
Design of the Optical Input System	45
VII. Encapsulants	47
VIII. Experimental Procedure	49
Sample Preparation	49
Profiling Procedure.	51
IX. Results.	53
Results from Silicon Implanted Samples	53
Results from Magnesium Implanted Samples . . .	55
X. Conclusion and Recommendations	66
Conclusions	66
Recommendations.	67
Bibliography	68
Appendix A: Plasma Deposition of Silicon Nitride Films	70

List of Figures

<u>Figure</u>	<u>Page</u>
1 General Scheme of Ion Implantation	8
2 Nuclear Collision in Laboratory Coordinate Systems	8
3 Nuclear Collision in Center of Mass (CM) Coordinate Systems.	12
4 Definition of the Total Range, R_{tot} , and the Projected Range, R_p	14
5 Typical Profile Predicted by the LSS Theory.	14
6 Glow Discharge	20
7 Sputtering Rate Determination.	27
8 Calibration Samples.	28
9 Result from Silicon Calibration Under 20 μ mHg and 2300V.	30
10 Result from Silicon Calibration Under 20 μ mHg and 2200V.	31
11 GDOS Systems	35
12 Sputtering Chamber	36
13 The Cathode.	37
14 Illumination of the Collimator Mirror through a Rectangular Slit	43
15 Optical Input System for GDOS.	44
16 Profile Obtained from SIMS of Silicon Implanted Gallium Arsenide	55
17 Typical Chart Outputs from GDOS.	56
18-23 Measured Profiles of Mg Implanted Gallium Arsenide	59-64
24 A Laboratory Plasma-Enhanced Chemical Vapor Deposition (PECVD) System.	73
25 A Radial Flow Reactor Design	73

List of Tables

<u>Table</u>		<u>Page</u>
I	Result from Silicon Calibration for 2300V Supply Voltage	29
II	Result from Silicon Calibration for 2200V Supply Voltage	29
III	Result from Determination of Si Concentration in a Bulk Doped GaAs Sample.	54
IV	Peak Concentrations and Distances into Si ₃ N ₄ film from 800°C annealed Mg Implanted GaAs . .	65
V	Properties of Silicon Nitride Film from SiH ₄ + NH ₃ Grown at 300°C	74

Abstract

An optical input system to an existing Glow Discharge Optical Spectroscopy (GDOS) apparatus was designed aiming to improve its sensitivity. The GDOS, unmodified, was used to obtain impurity concentration profiles of annealed and un-annealed ion implanted gallium arsenide samples. Implant energy was 120 KeV. Silicon ions were implanted with fluences of 5×10^{14} ions/cm², 1×10^{15} ions/cm², and 5×10^{15} ions/cm². Magnesium ions were implanted with fluence of 3×10^{15} ions/cm². Silicon implanted samples were encapsulated with aluminum nitride (AlN) films using a sputtering deposition technique. Magnesium implanted samples were encapsulated with 1000Å silicon nitride (Si₃N₄) films deposited by the plasma-enhanced chemical vapor deposition (PECVD) method. Samples were sputtered in a low pressure argon filled quartz chamber. Light emitted from elements of interest was monitored. Light intensity was converted to impurity concentration by comparison to the light intensity emitted by a standard sample of the same element. A summary of PECVD technique is given in Appendix I.

GLOW DISCHARGE OPTICAL SPECTROSCOPY OF ION IMPLANTED GALLIUM ARSENIDE

I Introduction

Background

There have been trends toward applications of III-V semiconductor materials, gallium arsenide for example. Such materials have higher electron mobility, wider band gap, and higher breakdown voltage than Germanium and Silicon. These properties make the materials ideally suitable for high frequency majority carrier devices, especially the microwave field-effect transistor (FET). The geometry of these devices is one micron or smaller. Doping by standard diffusion processes becomes very difficult mainly because of the lateral diffusion and dissociation of the crystal at high temperatures. Ion implantation is a better alternative.

Ion implantation, as compared to diffusion processes, offers very precise control over the spatial distribution of impurity atoms, namely impurity profiles. A profile can be completely introduced beneath the substrate surface, and it may be implanted in any order, instead of the collector-base-emitter sequence as it must be done with diffusion. This may give flexibility for some processing sequences. Moreover, ion implantation is a low temperature process.

The impurity profile is a complicated function of impurity ion energy, atomic numbers of both ion and target atoms, crystal orientation of the target, and ion fluence. The Lindhard-Scharff-Schiott theory (LSS) is the classic theory for prediction of the profiles (Ref 1).

Because the target is bombarded with high energy ions, radiation damage is an inherent problem in ion implantation. The damage alters the electrical and physical properties of the target material; therefore, it must be reduced. Annealing at certain temperatures, according to the material involved, has been found to reduce radiation damage to acceptable levels.

The Air Force Avionics Laboratory is very much interested in ion implantation of the III-V semiconductors. Work is being done on implanted gallium arsenide (GaAs) and indium phosphide (InP). The photoluminescence technique is used to identify impurity atoms and impurity energy levels.

Impurity profiles are measured by Glow Discharge Optical Spectroscopy (GDOS) and the Hall Coefficient measurement. The GDOS measures the physical profiles. However, only part of total impurity atoms are electrically active and only these are observed in the latter measurement. Secondary Ion Mass Spectroscopy (SIMS) and Auger Spectroscopy both provide very accurate measurements of the profile, but these systems are very complicated and require expensive and elaborate equipment. Differential capacitance-voltage (C-V) measurements,

when properly analyzed, also yield impurity profiles.

In GDOS, implanted samples are sputtered away in a DC glow discharge. In this process impurity ions emit radiation which is characteristic of the impurity element. The light intensity is proportional to the impurity concentration. Light is detected with a spectrometer as sputtering extends through a period of time. The result is a depth profile.

Objectives

Work on this thesis is a part of the continuing research by the Air Force Avionics Laboratory. Three specific objectives were set.

- i. To use the GDOS to measure and analyze implanted profiles and effects of encapsulant, especially plasma-deposited silicon nitride.
- ii. To investigate theoretical comparisons between plasma-deposited silicon nitride films for encapsulants versus films from other deposition techniques during annealing.
- iii. To design and implement modifications to existing GDOS apparatus to improve sensitivity.

Scope

It was recommended in reference 2 that the spectrometer be rotated by 90 degrees in order that the edge of the glow discharge could be imaged along the slit height, i.e. letting more light pass through the slit. This would be expected to

increase the sensitivity of the GDOS. It was proposed in this thesis that this be carried out plus a redesign of the existing optical system to the input slit based on principles of slit illumination.

The modified GDOS was then to be recalibrated and used to measure implanted silicon (Si) and magnesium (Mg) impurity profiles on chromium doped semi-insulating GaAs substrates. For Si, the implanted doses were 5×10^{15} , 1×10^{15} , and 5×10^{14} ions/cm² implanted at an energy of 120 keV. Two samples of 1×10^{15} ions/cm² were double implanted at an energy of 120 keV and 60 keV. A study of annealing was done only on the samples with 1×10^{15} ions/cm² dose; the annealing temperatures were 900°C and 750°C. For Mg, all samples were implanted with a dose of 3×10^{15} ions/cm² at an energy of 120 keV. Two unannealed samples were analyzed; all the rest were annealed at a temperature of 800°C for different lengths of time as follow: 1,2,4,8,15 and 25 minutes.

It was decided once the research was in progress that the research would be concentrated on only the plasma-deposited films instead of the original second objective. The films are presumed to be superior and are used as an encapsulant whenever possible at the Avionics Laboratory.

Results

This thesis was partially successful when measured against the objectives. Design of the optical input system was completed but was not implemented. Consequently, all profiles

had to be measured with the unmodified GDOS. Implanted silicon was not detected at all due to failure in the implantation process for the element. Unannealed Mg profiles agree closely with the profile predicted by the LSS theory. However, profiles were found to shift toward and off the surfaces of the substrates for annealing times of as short as one minute.

There was no evidence that physical properties of a plasma-deposited film are superior to others except for the advantage of being a lower temperature process.

Organization of Report

Section II of this report involves the history and theory of ion implantation. In section III, glow discharge is discussed in general, and in section IV GDOS and methods of obtaining impurity concentration are discussed. Section V details the GDOS equipment. The design of the optical input system is presented in section VI. Section VII deals with encapsulation. Section VIII presents the experimental procedure. Results are reported and discussed in section IX. Section X contains conclusions and recommendations. There is one appendix explaining the plasma film deposition technique.

II Ion Implantation

History

The origin of ion implantation sprang from the development of the nuclear reactor in the early 1940's (Ref 3:1-5). These reactions produce intense fluences of fast neutrons which must be shielded. To solve the problem, the theory of energetic ions penetrating matter was developed.

By this time the transistor had been invented and there was great interest in semiconductor materials. At first, the bombardment of semiconductors by atomic particles was considered only in that it deteriorated the materials. In 1952 Russell Ohe bombarded silicon point-contact diodes with helium ions; he obtained an improvement in the reverse current characteristics. In 1954 Shockley submitted a patent which clearly demonstrated his insight into applications of ion implantation. He proposed that the base of a junction transistor could be formed with a thickness of the order of a few microns. Ionic impurities of opposite doping type to that of the base doping impurity would be introduced to neutralize the base impurity to the desired depth. The first deliberate attempt to implant impurities into semiconductors was performed by W.D. Cussin in 1955. He implanted twelve different types of impurities, including boron, into both single-crystal and amorphous germanium and obtained p-type conductivity

which seemed to disappear after a 500°C anneal (Ref 4). He concluded that the principal effect of the bombardment was the disruption of lattice sites in germanium. The necessity of annealing out radiation damages was recognized by McCaldin and Widmer in 1963.

The Process

There are many variations, but the general nature of an ion-implantation scheme is shown in figure 1. Ions are emitted from a source. Next to the source is an accelerator which is biased with a high voltage opposite in polarity to the ions. The magnetic mass analyzer functions as a filter; it picks off only desirable ions and directs the beam into a beam sweeping, like that for the electron beam in an oscilloscope, so that the target area can be evenly implanted. Finally, at the end there is a target holder. The entire system is under vacuum.

Energy Loss Equations

As ions penetrate a target material, they dissipate energy and finally come to rest. In the LSS theory (Ref 4), there are two types of mechanisms, called stopping powers, by which ion energy is lost. Interactions between electrons of the ions and target atoms result in electronic stopping power whereas interactions between their nuclei are responsible for nuclear stopping power.

Electronic stopping power, S_e , is based on the stopping properties of a free electron gas. Energy of the incident

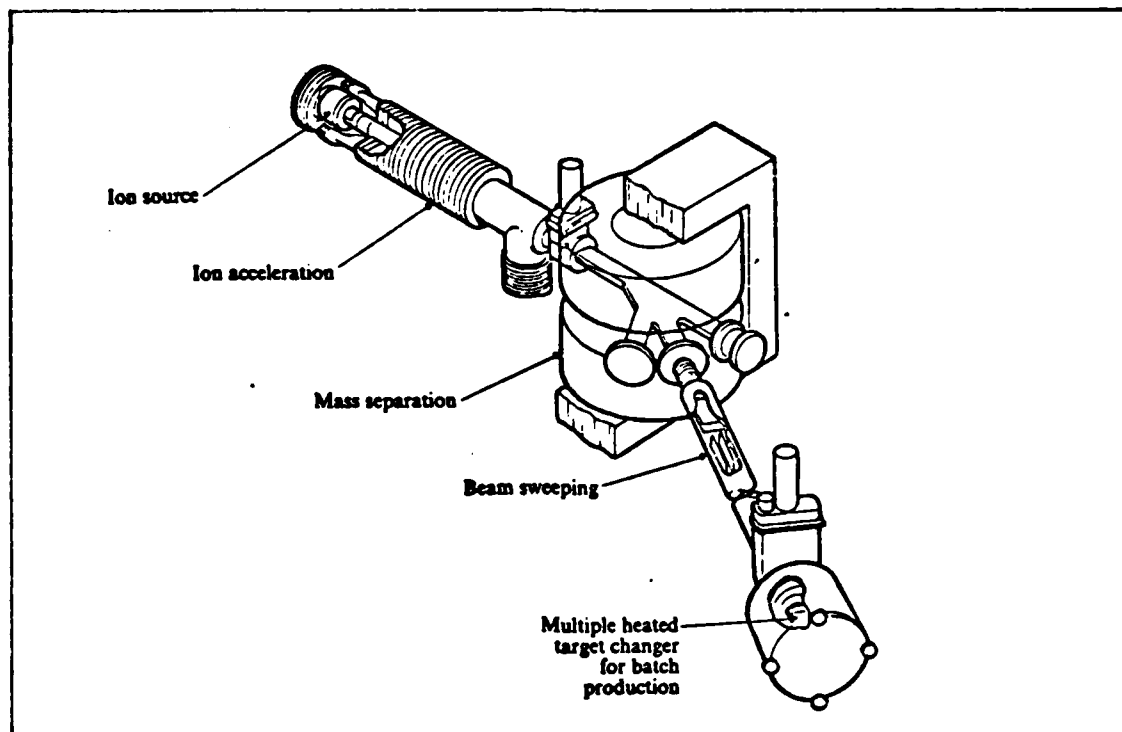


Figure 1. General Scheme of Ion Implantation. (Ref 20)

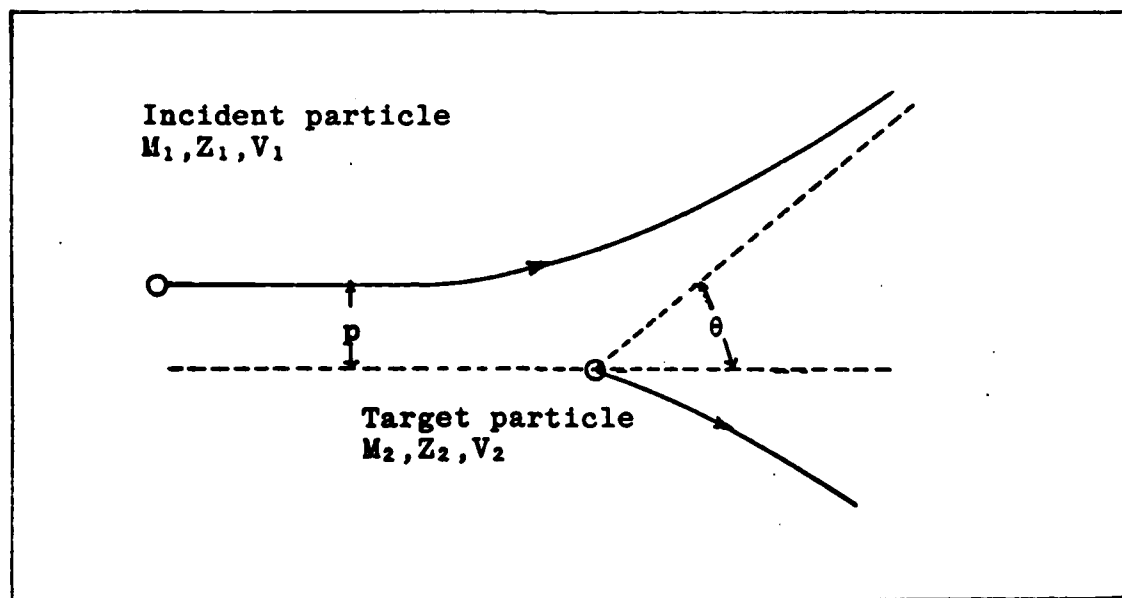


Figure 2. Nuclear Collision in Laboratory Coordinate Systems (Ref 4).

ion is lost by close collisions with electrons and by excitation of a plasma resonance in the free electron gas at points that are distant from the ion trajectory (Ref 4). Lindhard and Winther assume that S_e is proportional to the velocity of the ions or to the square root of ion energy (Ref 4)

$$S_e(E) = kE^{\frac{1}{2}} \quad (1)$$

$$k = (k' C_R) / C_E^{\frac{1}{2}} \quad (2)$$

$$k' = \frac{0.0793 z_1^{\frac{1}{2}} z_2^{\frac{1}{2}} (A_1 + A_2)^{\frac{3}{2}}}{(z_1^{\frac{2}{3}} + z_2^{\frac{2}{3}})^{\frac{3}{4}} A_1^{\frac{3}{4}} A_2^{\frac{1}{4}}} \quad (3)$$

$$C_R = \frac{4\pi a^2 M_1 M_2}{(M_1 + M_2)^2} \quad (4)$$

$$C_E = \frac{4\pi \epsilon_0 a M_2}{z_1 z_2 q^2 (M_1 + M_2)} \quad (5)$$

where

z_1 = atomic number of impurity atom

z_2 = atomic number of target atom

M_1 = mass of impurity atom

M_2 = mass of target atom

A_1 = atomic weight of impurity atom

A_2 = atomic weight of target atom

q = electronic charge (1.602×10^{-19} C)

ϵ_0 = free space permittivity

a = screening parameter

Equation (1) is valid when the velocity of the ions is below the velocity of an electron whose energy is equal to the Fermi energy of the electron gas.

Nuclear stopping power, $S_n(E)$, is due to the scattering process. Ion energy is lost through direct and indirect collisions. It is the energy lost to target nuclei when a projectile (ionic particle) of energy E traverses a differential thickness Δx of a target of unit density (Ref 4).

It is assumed that each nucleus in the target independently contributes to the collision. A projectile, as sketched in figure 2, approaches a target nucleus along a path parallel to the head on collision path. The distance between these two lines is the impact parameter, denoted by p . As a projectile encounters the repulsive potential, $V(r)$, of the target, it transfers energy, T , to the target and its path is deflected by an angle θ . The transferred energy is then determined by the initial energy of the projectile, E , and p . Energy lost due to interaction with all nuclei as the projectile travels a distance Δx is (Ref 4)

$$\Delta E = -N\Delta x \int_0^\infty T 2\pi p dp \quad (6)$$

where N = density of the target material.

Taking the limit of $\Delta E/\Delta x$ as Δx approaches zero, $S_n(E)$ is the integral

$$S_n(E) = \int_0^{\infty} T(E,p) 2\pi p dp \quad (7)$$

The calculation is customarily done in the center of mass coordinates (CM) as shown in figure 3.

If the collision is assumed to be elastic, then total energy and momentum of the system is conserved. The scattering deflection angle, ψ , can be expressed as

$$\psi = \pi - 2p \int_0^{u_{\max}} du (1 - V(u)/E_r - p^2 u^2) \quad (8)$$

where

$u = 1/r$, with r being the distance between the particles in the CM coordinate system.

$V(u)$ = interaction potential function.

E_r = energy of projectile in CM coordinate system ($E_r = EM_r/M_1$)

M_r = reduced mass = $(M_1 M_2)/(M_1 + M_2)$

u_{\max} satisfies the equation $1 - V(u_{\max})/E_r - p^2 u_{\max}^2 = 0$

Basically $V(u)$ is the Coulomb potential. There is a shielding effect by electrons when p is large; therefore, the interaction potential must be modified.

$$V(r) = z_1 z_2 q^2 f(r/a)/(r\pi\epsilon_0 r) \quad (9)$$

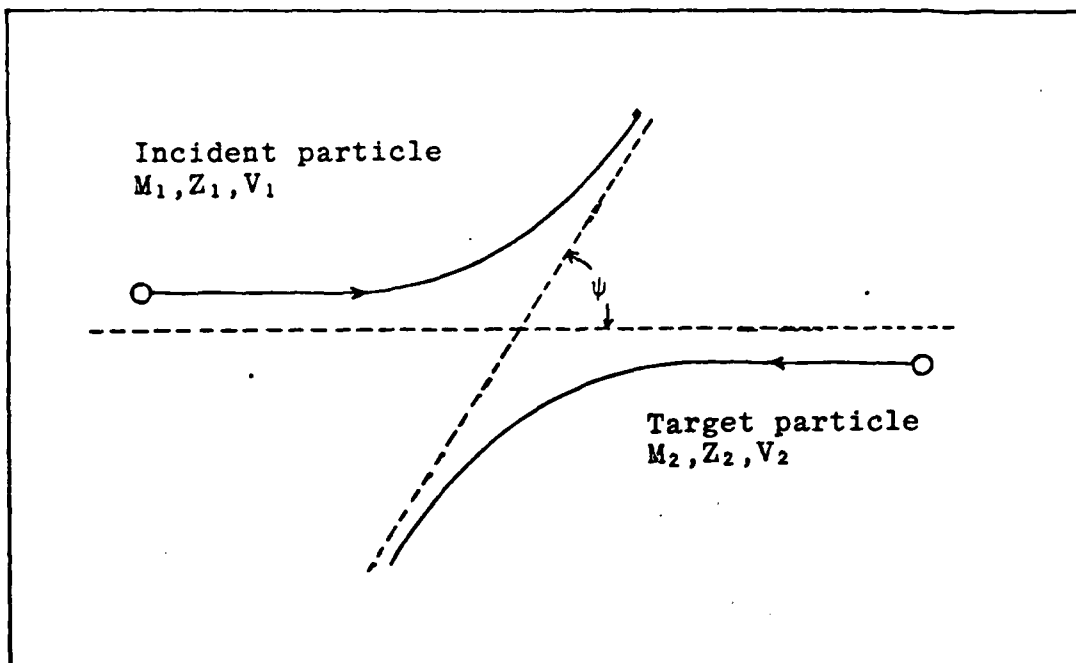


Figure 3. Nuclear Collision in the Center of Mass (CM) Coordinate System. (Ref 4).

where $f(r/a)$ = the screening function and a = the screening parameter.

Transformation from the CM coordinate system to the laboratory coordinate system yields the relationship between θ and ψ ,

$$\tan\theta = (\sin\psi)/(\cos\psi + M_1/M_2) \quad (10)$$

The relationship between θ and T is

$$\cos\theta = |1 - (1+\mu)T/2E|/(1-T/E)^{1/2} \quad (11)$$

Equations (8) through (11) give the relationship between T , E , and p ; the integral in equation (7) can now be

evaluated.

The energy loss equation is,

$$dE/dx = -N(S_n(E) + S_e(E)) \quad (12)$$

Electronic stopping power predominates for light ion, high energy implantation such as magnesium (Ref 2).

Ion Range Distribution

The total distance that the projectile travels until it comes to rest is called total range, R_{tot} . The projection of R_{tot} along the incident direction is called the projected range, R_p . The more important quantity is R_p since it can be observed directly. Figure 4 defines both R_{tot} and R_p .

The total range can be calculated by integration of equation (12) over the limit from initial energy, E , to zero.

$$R_{tot} = \int_E^0 \frac{dE}{dE/dR}$$

or

$$R_{tot} = 1/N \int_0^E dE (S_n(E) + S_e(E)) \quad (13)$$

The relationship between R_{tot} and R_p is given in reference (1) as,

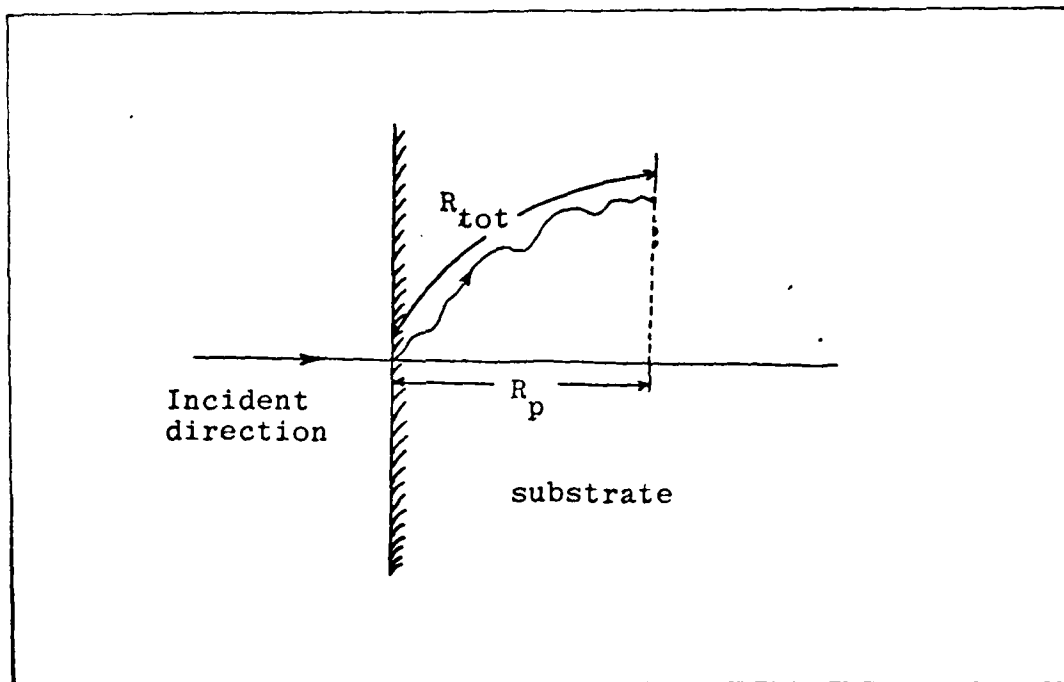


Figure 4. Definition of the Total Range, R_{tot} , and the Projected Range, R_p (Ref 4).

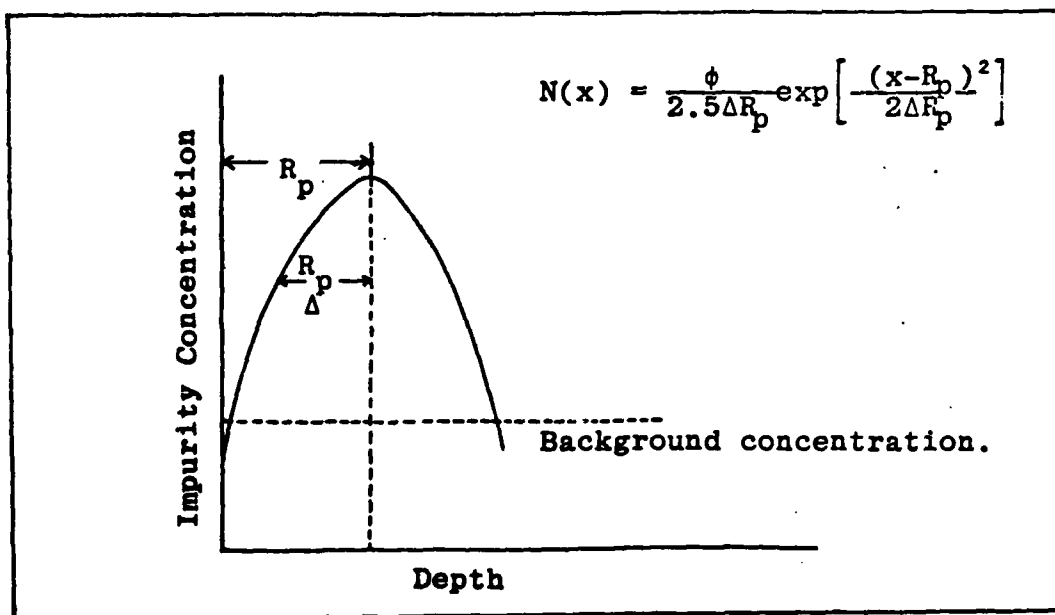


Figure 5. Typical Profile Predicted by the LSS Theory

$$R_{\text{tot}}/R_p = \frac{1}{4} \left| -1 - 3\mu + (5 + \mu) \frac{1 + \mu}{2\mu^{\frac{1}{2}}} \arccos \frac{1 - \mu}{1 + \mu} \right| \quad (14)$$

where $\mu = M_2/M_1$.

When nuclear stopping power dominates, equation (14) is approximately (Ref 5:25)

$$R_{\text{tot}}/R_p \approx 1 + \mu/3 \quad (15)$$

Because of the randomness in the scattering process, impurities scatter about R_p and the profile is approximately a Gaussian distribution as shown in Figure 5. Measurement of the deviation from R_p is called the projected range straggling, denoted by ΔR_p . The impurity profile is given as (Ref 5:32)

$$N(x) \approx \frac{\phi}{2.5\Delta R_p} \exp \left| -\frac{(x - R_p)^2}{2\Delta R_p^2} \right| \quad (16)$$

where ϕ is the fluence (number of ions/unit area).

The maximum concentration of impurities at depth R_p is then,

$$N_p \approx \frac{\phi}{2.5\Delta R_p} \quad (17)$$

The projected range and the straggling have been calculated and tabulated in many references for various pairs of ion and target materials. Reference 6 concerns implantation of different ions in solids in general; reference 7

specifically deals with semiconductor implantation. Both references also give information on the radiation damage distributions which will be discussed shortly.

The theory of ion range distribution discussed above is applicable only when the target is amorphous. For a crystalline or single crystal material target, channelling occurs.

Channelling in Single Crystal Materials

Different planes of a single crystal have different reflection indices because of the crystal structure itself. A diamond structure appears to be more dense along the $\langle 100 \rangle$ axis than it does along the $\langle 110 \rangle$ axis, has open tubes or channels through its thickness. The potential of the string of atoms, acting like a potential wall, steers an ion much deeper into the target than a normal range from random collisions. The channelled ion will eventually come to rest due largely to $S_e(E)$, and partially due to $S_n(E)$ of the interstitial atoms.

If an ion enters the target closer to the potential wall than a critical radius, it undergoes the random scattering process. This is due to the fact that momentum transfer is large for small p . The critical distance occurs at the point at which energy from the potential wall equals the transverse energy of an ion i.e. the energy component perpendicular to the incident direction. The Linhard model superimposed the range distribution of channelled ions and randomly scattered ions. A typical impurity profile contains two peaks; the peak due to scattering is closer to the target

surface than the one which is due to channelling.

The practical application of channelling may be in a low-energy, deep penetration implantation (Ref 5:46). However, in most cases channelling is undesirable and must be prevented. Dechannelling is accomplished by the following techniques (Ref 8):

- a. Adjusting the incident beam away from the axis along which channelling easily occurs. The angles used to dechannel silicon, for example, are 5.2° , and 4.0° with respect to the $\langle 110 \rangle$ and the $\langle 100 \rangle$ axes, respectively.
- b. Heating the target to increase lattice vibration, hence increasing the chance for random scattering.
- c. Growing oxide at the surface to initiate random scattering.

Radiation Damage and Annealing

Radiation Damage is caused by energy dissipation from ions. Energy in excess of a maximum value of about 25eV, called the displacement energy, can permanently displace a lattice atom from its site (Ref 3:154). The two most important defects are interstitial atoms and vacancies. Interstitials are characterized by extra atoms in the normal lattice. A vacancy is the absence of an atom from its lattice site. The spatial distribution of radiation damage is similar to that of the ion distribution except that it peaks

nearer the target surface (Ref 5:39-43).

In implanted semiconductors, radiation damage is often high enough to disrupt the crystal lattice and turn the semiconductor into an amorphous material. This changes both physical and electrical properties of semiconductors and this damage must be reduced. Removal of the damage is accomplished by thermal annealing. Amorphous silicon, under electron microscope studies, was shown to recrystallize at a temperature of about 650°C. The crystal structure was recovered by epitaxial growth onto the undamaged layer. Annealing temperatures of Ge and GaAs are 400°C and 250°C respectively (Ref 3:195-199). Although annealing does not restore all damage, it reduces residual defects to a level where the implanted semiconductors are useful.

III Glow Discharges

Glow Discharges

Light is emitted from a plasma at characteristic wavelengths determined by the energy differences through which electrons fall as excited atoms or molecules relax to less excited states. These emission spectra can be used to identify the constituents of the plasma.

Noble gas molecules contained in an evacuated chamber with two electrodes can be ionized by a strong DC electric field provided by a DC voltage on the order of 0.5 to 5 kV (Ref 9). The photons given off form a visible column between the electrodes. The column includes seven regions as shown in Figure 6. The following description (Ref 19:124-132) pertains to a self sustaining discharge. In such a discharge, electrons, liberated by ion bombardment of the cathode, ionize gas molecules which in turn bombard the cathode and liberate the same number of electrons from the cathode. Figure 6 illustrates the following regions of a Glow Discharge:

- a. Aston dark space. Electrons emitted from the cathode do not have sufficient energy to ionize or excite the gas molecules while ions rush to the cathode with such a high velocity that their chance to be neutralized is low. There is virtually no light emitted except from that fraction of ions which

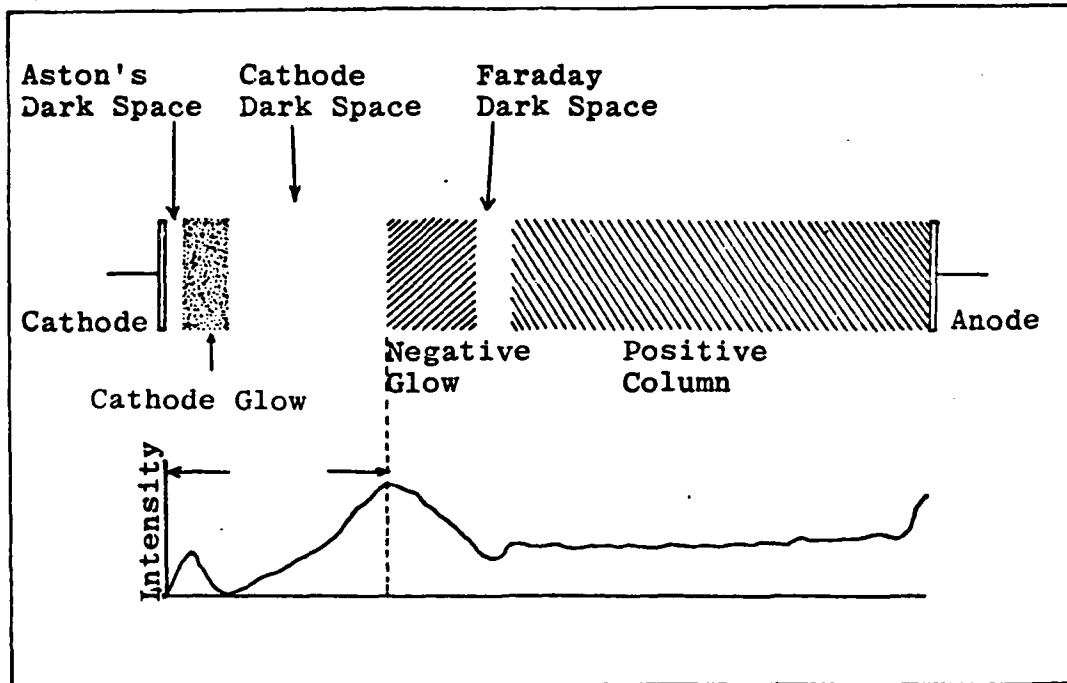


Figure 6. Glow Discharge (Ref 2)

enter the region in an excited state.

- b. Cathode glow region. The electrons acquire sufficient energy to excite ions. The intensity is maximum. Most electrons collide and lose almost all their energy.
- c. Crookes dark space. Electrons which do not collide in the last region ionize the gas here, but newly generated electrons, called secondary electrons, do not have sufficient energy to excite ions. Consequently, this region emits very little light. Identified as cathode dark space in Figure 6).
- d. Negative glow region. The secondary electrons have

enough energy to excite ions; therefore, large numbers of photons are emitted.

- e. Faraday dark space. The cause for the lack of photon emission is the same as that of the Crookes dark region. However, the electric field in this region is small, so electrons do not regain much energy.
- f. The positive column. This region, an example of a plasma, is more luminous than the Faraday dark space. It does not appear if the space between electrodes is too small.

The first four regions together are called the cathode fall. This is the region across which the largest voltage drop occurs. Glow discharge processes involve this region.

Sputtering

As described above, there is constant emission of electrons and ions from the cathode while the glow discharge is sustained. The cathode is being etched by this emission of electrons and ions. This etching process is called sputtering. In general, the sputtering process is one in which a target is etched away by continual ion bombardment. Sputtering is a function of many variables including the masses of the ion and the target atom, the ion energy, direction of ion incidence to the face of the target, the target temperature and the ion flux (Ref5:111). There is some threshold energy below which sputtering does not occur; however, if the energy is too

high, the sputtering yield decreases due to deep penetration (Ref 10:194).

Atoms are ejected preferentially along the $\langle 111 \rangle$ and $\langle 100 \rangle$ directions in a diamond lattice like silicon (Ref 11). Most ejected particles are in an electrically neutral state (Ref 2). Cooper et al. (Ref 12) sputtered GaAs under 2×10^{-3} torr of argon gas and 100V negative voltage supply; they measured the number of molecules ejected per ion to be 0.169 and 0.159 for the $\langle 111 \rangle$ and $\langle \bar{1}\bar{1}\bar{1} \rangle$ directions respectively.

IV Glow Discharge Optical Spectroscopy (GDOS)

Principle

An individual photon emitted in the glow discharge corresponds to a single wavelength. The relationship is

$$E = \frac{hc}{\lambda} \quad (18)$$

where

E = photon energy

h = Planck's constant

c = velocity of light

λ = wavelength

The fact that made GDOS possible is that each element has its own unique set of photon energies associated with transitions between states. The composition of the cathode material can be identified from the corresponding wavelengths in the emission spectrum.

It should be intuitively clear that the concentration of an element being detected is proportional to the intensity of the corresponding light. Unfortunately, the relationship between the two quantities is very complicated. It depends on the sputtering rate which in turn depends upon sputtering conditions, cathode geometry, and the cathode material. This makes direct calibration of GDOS extremely

difficult if not impossible. However, there is a much easier alternative. By using a standard material as the cathode and comparing the intensity of the emitted light to that observed from the compound, the proportionality constant can be determined, provided that the sputtering rate and conditions are identical in both cases.

Determination of Impurity Concentration

The number of photon counts per second is taken to be linearly proportional to the number of impurity atoms contained in the volume being sputtered in one second.

$$M = kNV \quad (19)$$

where

M = number of photon counts/second

N = concentration (atoms/cm³)

V = volume being sputtered in one second (cm³/sec)

k = constant of the system

Hidden in the constant, k , are the loss of light in the system, the number of ionized impurities, and fraction of ionized impurities which relax. Under the same sputtering conditions, k is fixed for every measurement.

In equation (19), V may be expressed in terms of sample area and sputtering rate as

$$M = kNA\beta \quad (20)$$

where

A = sample area (cm^2)

B = sputtering rate (cm/second)

For a standard element,

$$M_s = kN_s A B_s \quad (21)$$

For a sample with impurities

$$M_i = kN_i A_i B_i$$

where

$A_i = A_s$ for all measurements

but $B_i \neq B_s$ for all measurements

Then

$$\frac{M_i}{M_s} = \frac{N_i B_i}{N_s B_s} \quad (24)$$

Or

$$N_i = \frac{N_s B_s}{M_s B_i} M_i \quad (25)$$

Define the proportional constant C ,

$$C = \frac{N_s B_s}{M_s B_i} \quad (26)$$

The units of C are atoms/ $(\text{cm}^3\text{-count})$. The sputtering rate ratio must be kept as close to unity as possible, and the sputtering rates should be low in order to obtain accurate measurements.

Sputtering Rate Determination

A small square piece of gallium arsenide was placed on top of each sample to be sputtered. The piece prevented the part of the sample which it covered from being sputtered leaving an island as shown in Figure 7. The sputtering depth was measured with a Sloan Dektak Surface Measuring System. The Dektak was capable of measuring step heights from 25 to 1,000,000Å. The sputtering rate equals the depth divided by total sputtering time in seconds.

GDOS System Calibration

The purposes of the calibrations are to determine the proportionality constant and the linearity with respect to sputtered volume. Four square samples of different sizes (areas) were prepared from a wafer of pure silicon. Width of the largest sample was 0.5cm ; the others were $\frac{3}{4}$, $\frac{1}{2}$, and $\frac{1}{4}$ the area of the largest one. To keep the electric field in the discharge from varying, the geometry of the cathode had to be fixed. This was accomplished by placing four pieces of gallium arsenide on the perimeter of each sample. The pieces were prepared such that the total area of the silicon sample and the four pieces of gallium arsenide was 0.49cm^2 (see Figure 8).

Each sample was sputtered under different conditions. The results are tabulated in Table I and Table II. The average number of photon counts per second are plotted against

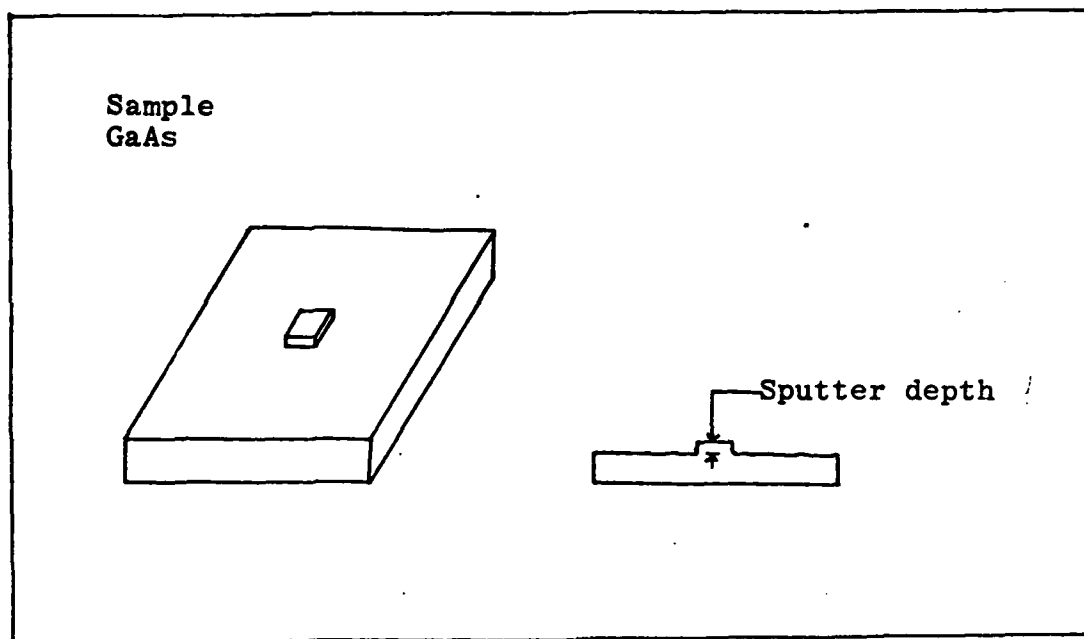


Figure 7. Sputtering Rate Determination

the nominal area in Figures 9 and 10. The number of counts linearly increases with area, hence with volume. Also, it is larger by 10% when the applied voltage is increased from 2200 to 2300 V.

The proportionality constant, C , was determined for the largest sample. The sputtering rate of pure silicon was $1334\text{\AA}/\text{min}$. The sputtering rate of implanted gallium arsenide was approximately $1150\text{\AA}/\text{min}$ (Ref 2). The sputtering pressure and voltage were 20 micron and 2200V respectively. Equation (21) yields,

$$C = \frac{5.0 \times 10^{22} \text{ atoms/cm}^3 \cdot 1334\text{\AA}/\text{min}}{95,875 \text{ counts} \cdot 1150\text{\AA}/\text{min}}$$

$$= 6.0 \times 10^{17} \text{ atoms}/(\text{cm}^3 \text{-count})$$

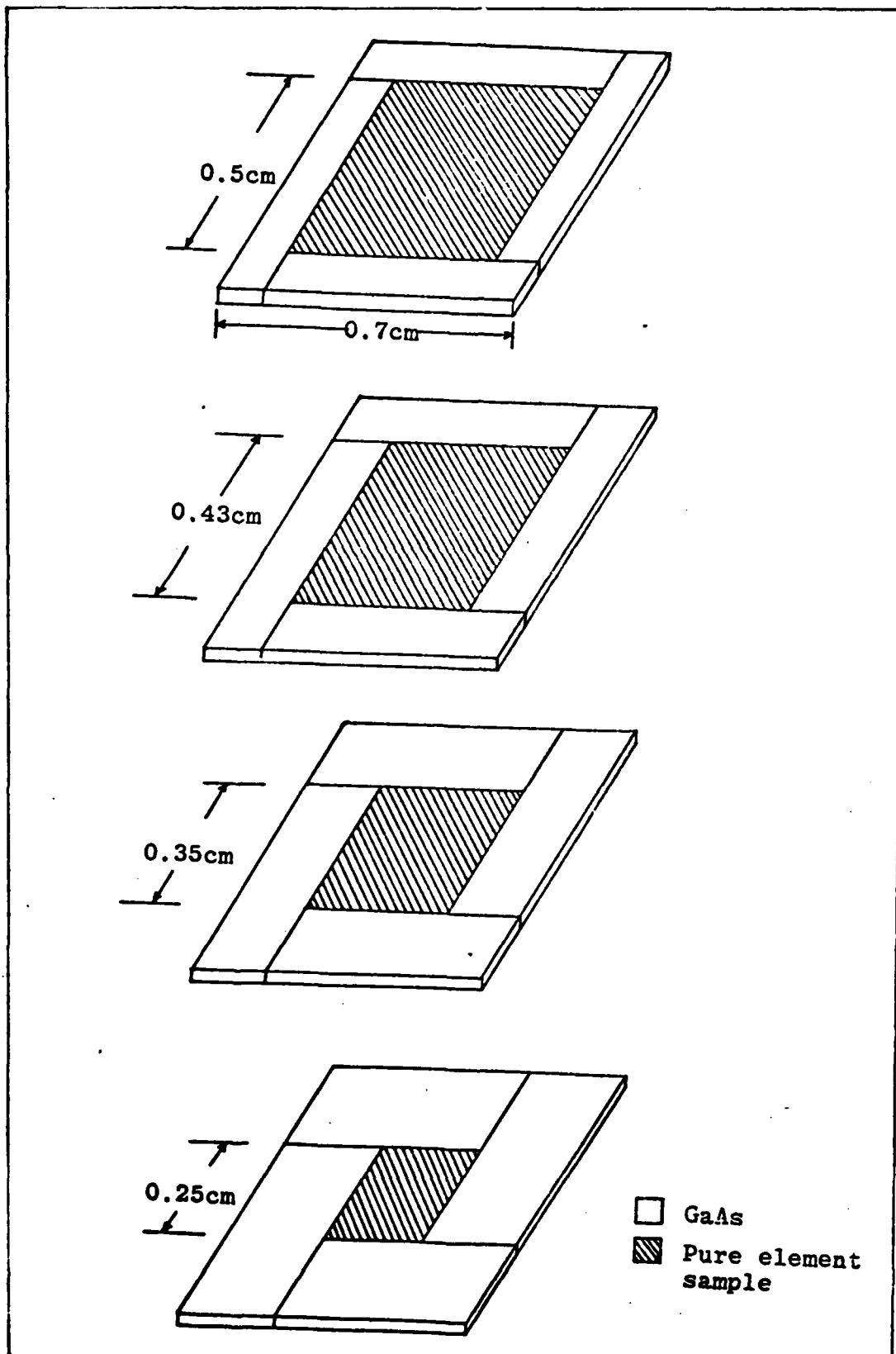


Figure 8. Calibration Samples

Table I

Results from Silicon Calibration
for 2300V Supply Voltage

Area (normalized)	Pressure (μ Hg)	Number of Photon Counts	Average Counts
1	19.0	96,500	111,500
	20.0	109,000	
	21.0	129,000	
3/4	19.0	79,200	89,733
	20.0	90,000	
	21.0	100,000	
1/2	19.0	53,000	60,333
	20.0	60,000	
	21.0	68,000	
1/4	19.0	30,100	33,775
	20.0	33,000	
	21.0	37,000	

Table II

Results from Silicon Calibration
for 2200V Supply Voltage

Area (normalized)	Pressure (mHg)	Number of Photon Counts	Average Counts
1	19.0	81,500	96,500
	20.0	94,000	
	21.0	114,000	
3/4	19.0	64,200	74,733
	20.0	75,000	
	21.0	85,000	
1/2	19.0	44,000	50,333
	20.0	50,000	
	21.0	57,000	
1/4	19.0	24,700	27,800
	20.0	27,500	
	21.0	31,000	

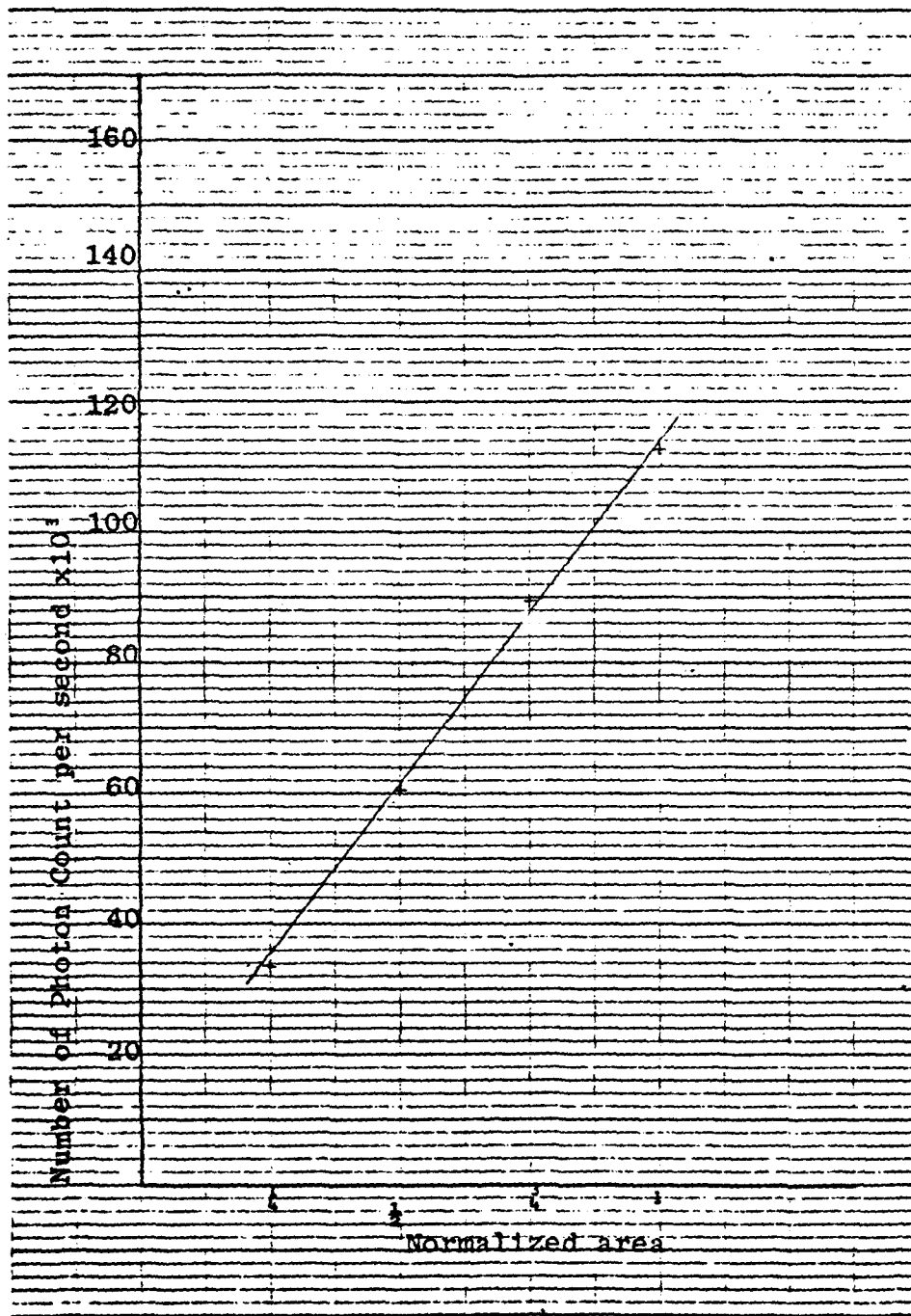


Figure 9. Results from Silicon Calibration Under 20 μ mHg and 2300V.

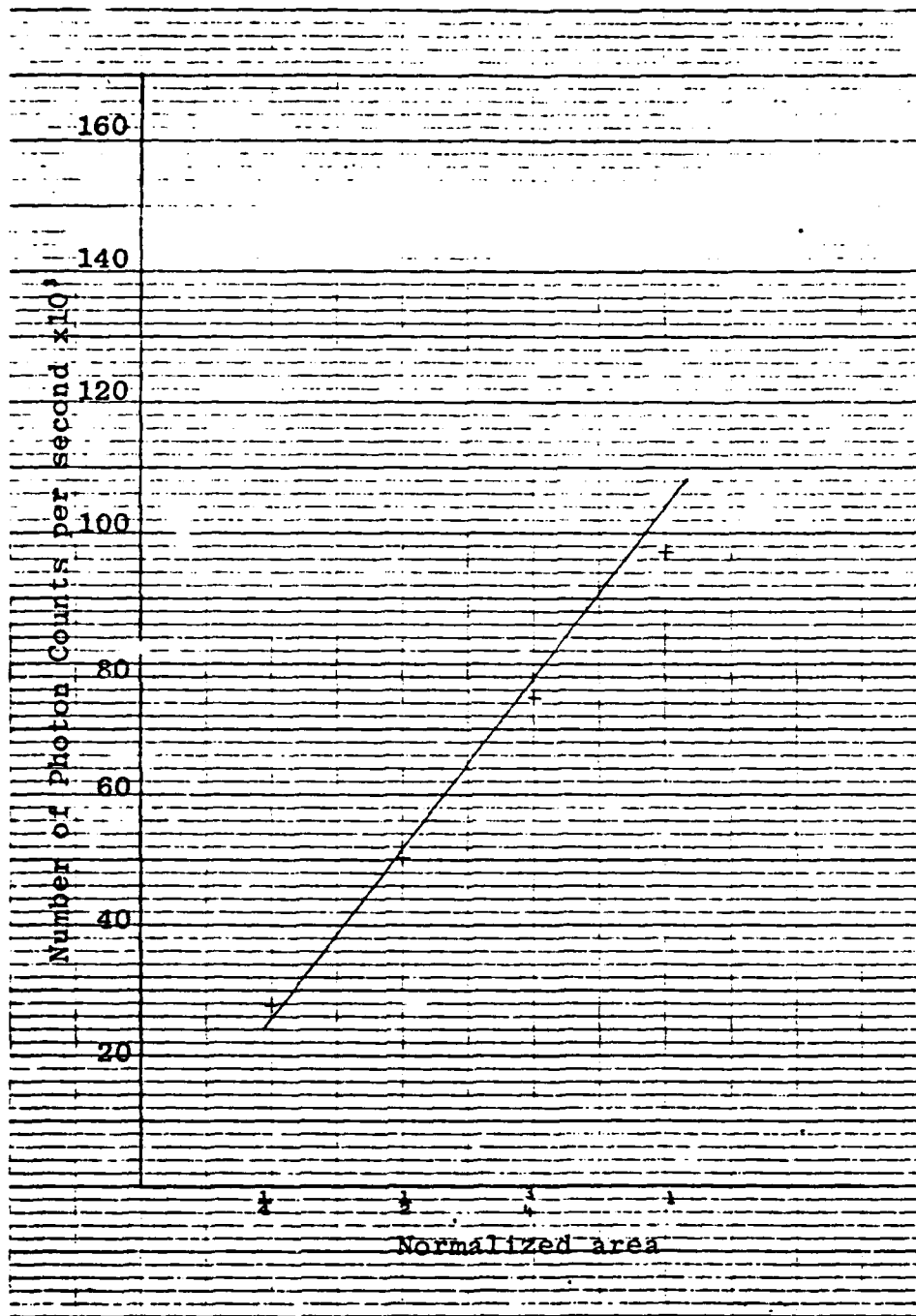


Figure 10. Results from Silicon Calibration Under 20 μ mHg and 2200V.

The calibration for magnesium in reference (2) was done by placing the magnesium sample directly on top of the cathode. Consequently, the electric field configuration was distorted due to the fact that magnesium is a metal. As a result, the sputtering rate of a pure magnesium sample was much higher than that of the magnesium implanted sample. In recalibration, a gallium arsenide sample, which is a dielectric, was placed between the magnesium sample and the cathode. Only one sample with area of 0.25cm^2 , was sputtered under $20\text{ }\mu\text{mHg}$ pressure and 2200V voltage supply. It was assumed that the linearity with respect to volume holds. The recorded number of photon counts was 55,000.

It was very difficult to measure the sputtering rate. The sample was mechanically polished, so the step could not be measured with a Dektak, and the sample was too thin to yield any measurable step. The sputtering rate was assumed to be equal to $1150\text{\AA}/\text{min}$ which is the rate for implanted gallium arsenide.

The proportionality constant was calculated using equation (21).

$$C = \frac{N_s B_s}{M_s B_i}$$

$$N_s = \frac{1.74\text{g}/\text{cm}^3}{24.312\text{amu}} \times \frac{1\text{amu}}{1.659 \times 10^{-24}\text{g}}$$

$$= 4.31 \times 10^{22} \text{ atoms/cm}^3$$

$$C = \frac{4.31 \times 10^{22} \text{ atoms/cm}^3}{55,000 \text{ counts}}$$

$$= 7.84 \times 10^{17} \text{ atoms}(\text{cm}^3\text{-count})$$

V Experimental Apparatus

A schematic diagram of the GDOS system used in this experiment is shown in Figure 11. The following description closely follows those in reference 2 because the same equipment is involved. The equipment is divided into three categories for descriptions:

1. Sputtering chamber assembly
2. Vacuum, gas, and cooling systems
3. Detecting and recording systems

Sputtering Chamber Assembly

A side view of the sputtering chamber is shown in Figure 12. The chamber is made from a 3 inch diameter, 6 inch high pyrex glass cylinder placed such that its axis is vertical. There are three open ports halfway from the top; two of them are in line but opposite each other. The third one is perpendicular to the line. Each port extends $4\frac{1}{2}$ inches from the center and is covered with a silica quartz window to allow ultraviolet light transmission. The third open port is used for monitoring the substrate; it is 2 inches in diameter. The first two ports are used for monitoring the impurity; they are $2\frac{3}{4}$ inches in diameter. At one end there is a $2\frac{1}{2}$ inch diameter collecting lens; a 3 inch diameter spherical mirror is placed at the opposite end to reflect

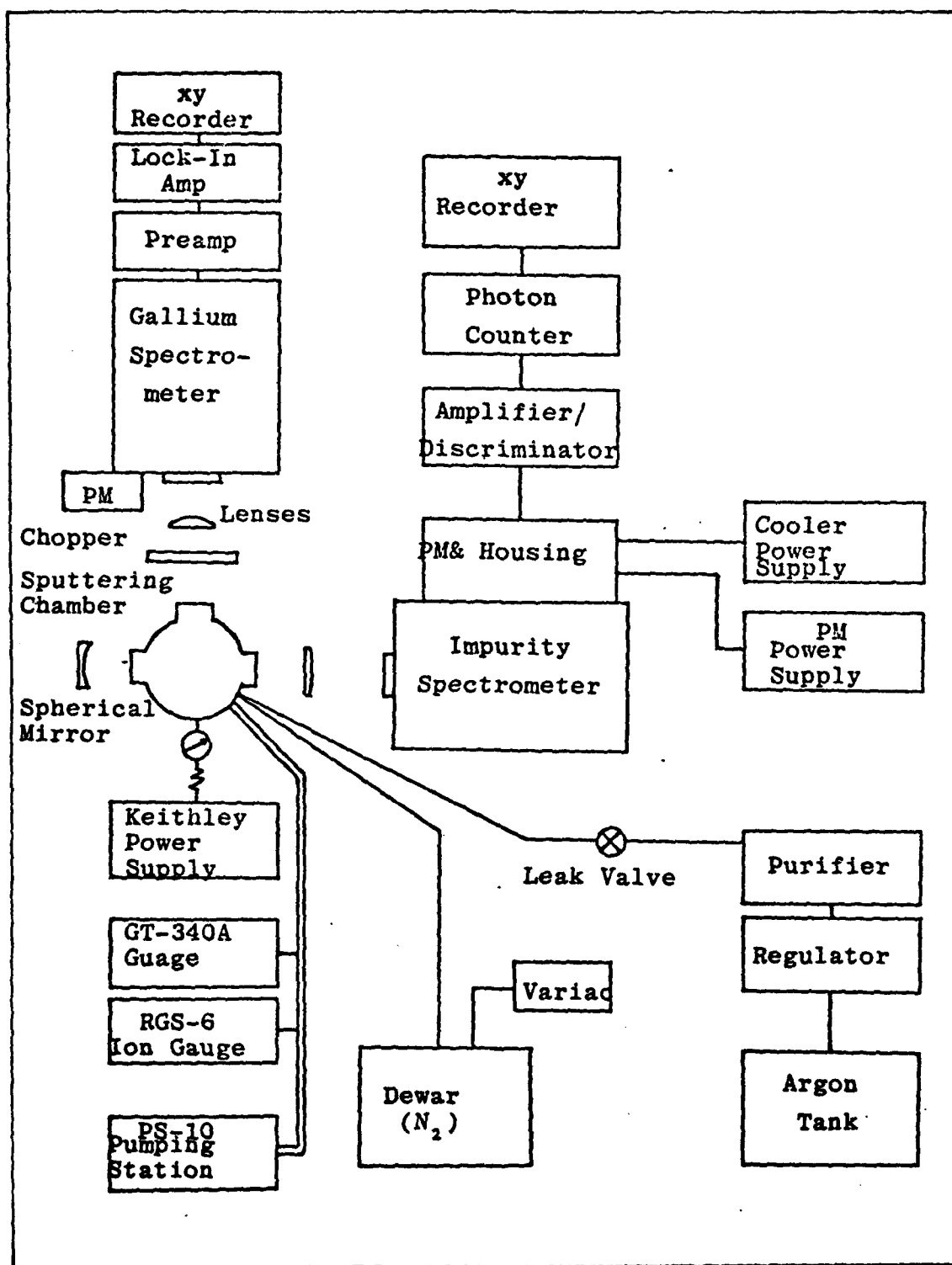


Figure 11. GDOS Systems. (Ref 2)

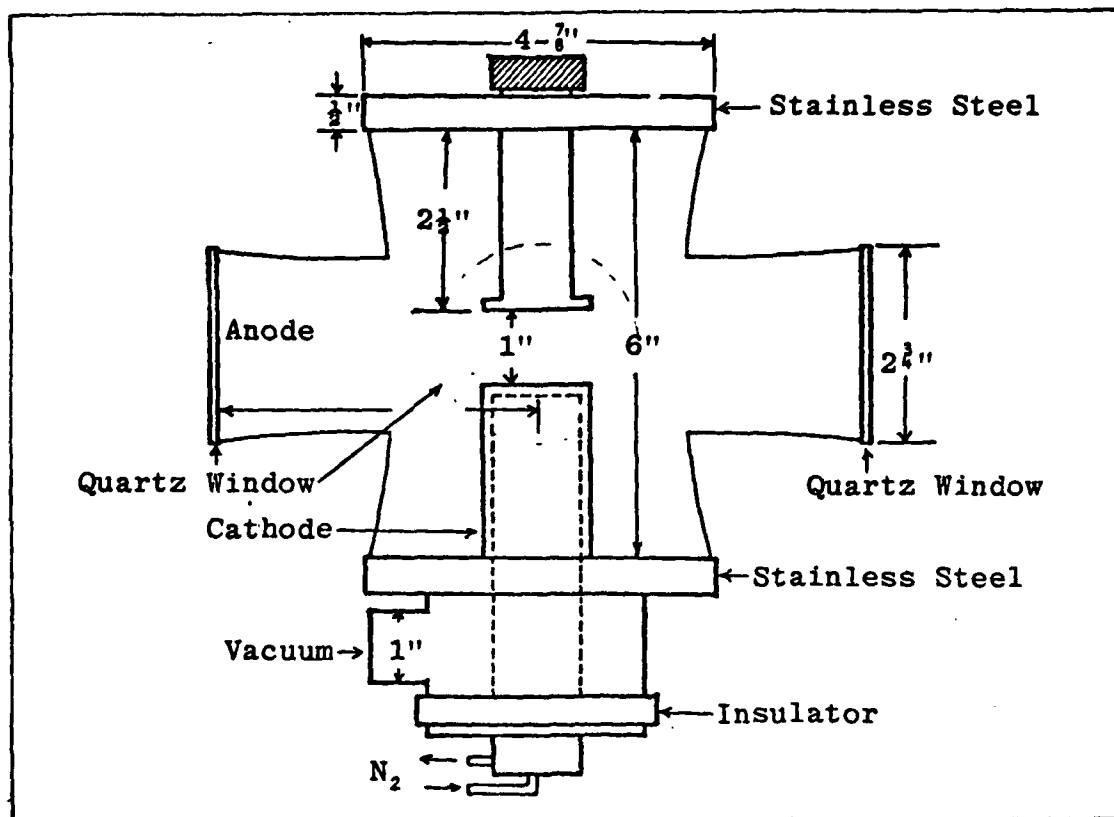


Figure 12. Sputtering Chamber (Ref 2)

more light to the lens.

The chamber is sealed with 1/8 inch thick rubber gaskets which are countersunk in grooves and by 1/2 inch thick stainless steel top and bottom plates. Extending downward from the center of the top plate is the anode. It has a 1 inch diameter, 2 1/2 inch long shaft with a 1 1/2 inch diameter cylindrical stub at the tip. The anode and the bottom plate are grounded.

A drawing of the cathode is shown in Figure 13. The cathode extends upward through the bottom plate to within an inch of the anode. It has a machined aluminum cap with a 1/2 inch diameter circular step. The active area of the cathode is a 1/2 inch diameter circular tungsten plate glued on the step. The whole cathode, except for the active area, is

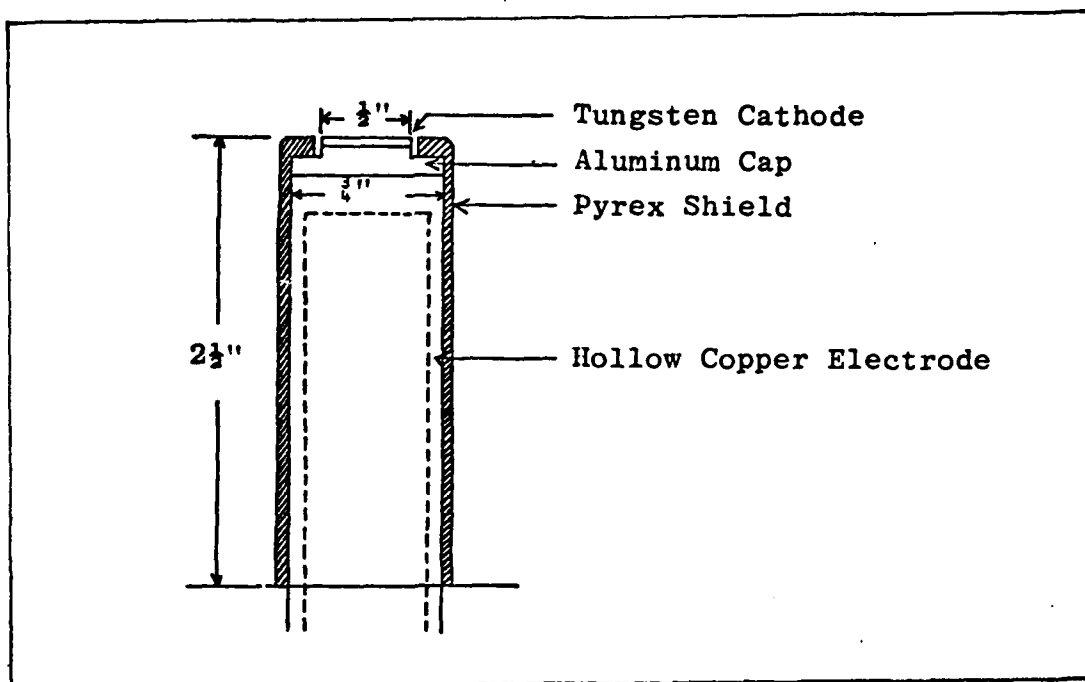


Figure 13. The Cathode (Ref 2)

covered with a closely fitting pyrex glass shield to prevent arcing. The cathode is cooled by nitrogen gas through a line that goes in and out of the cathode hollow part. The lower electrode assembly is fitted with a vacuum port and a thermocouple gauge.

The cathode is connected to a negative high voltage source. The voltage source was supplied by a Keithley Instruments Model 242 Regulated High Voltage Supply, with a range of $\pm 3500\text{V}$ at 25mA . A protective $160\text{k}\Omega$ resistor ne work is connected between the supply and the cathode. It protects the power supply in case of an accidental short-circuit and it limits ion current. Also connected in this circuit is a DC milliammeter used to monitor ion current.

Vacuum, Gas, and Cooling System

A Varian Model PS-10 Pumping Station is used to evacuate the sputtering chamber. The station has one mechanical pump and an oil diffusion pump. The mechanical pump is used first to provide a medium vacuum ($10\mu\text{mHg}$) . This phase is called rough pumping. Then it is switched to the back pumping mode to assist the diffusion pump which brings the pressure in the chamber down to $3 \times 10^{-5} \mu\text{mHg}$. A cold trap in series with the diffusion pump is cooled by liquid nitrogen. Medium vacuum is measured with a Model GT-340A Thermister gauge supplied by CVC Products Inc. connected to the thermocouple on the cathode assembly. High vacuum is measured with a Veeco Instruments RGS-6 Ionization Gauge Control with a RG75P ion gauge.

Argon gas is supplied to the chamber through a Hydrox Purifier Model 8301. The gas is approximately 99.9 percent pure argon. Flow rate of the gas is controlled with a lead valve manufactured by Granville-Phillips Co.

Cooling of the cathode is accomplished by nitrogen gas from a ten filter Dewar container. Liquid nitrogen in the container is heated by a submersed heating element. Nitrogen flow rate is controlled by a Variac auto transformer, which controls the amount of heat. The gas pipe to the cathode is a teflen tube.

Detecting and Recording Systems

There are two independent systems for detecting light and recording electrical output. One is used to monitor the impurity and the other is used to monitor gallium in the substrate. The second system is necessary because it provides data to be used in determining the point where the encapsulant film-to-substrate interface occurs.

For the detection of the impurity, light is gathered and focused by the collecting lens to the entrance slit of a spectrometer. The spectrometer is a Spex Industries Model 1704 one meter Czerny-Turner Scanning Spectrometer equipped with a 1200 lines/mm ruled, 3000Å⁰ blazed Bausch and Lomb diffraction grating. Light of selected wavelength, which is tuned by turning the grating plane, is focused through the exit slit. The widths of the entrance and exit slits are adjustable and are set at 200 and 400 µm respectively. The slits are 20mm high.

The light output from the exit slit is detected with an RCA C31034 eleven-stage Quantacon photomultiplier tube. The tube has a 2 inch ultraviolet transmitting window and a gallium arsenide photocathode. A typical amplification of the tube is $6 \times 10^{+5}$ when it is fully cooled by a PAR Model TE-104 thermoelectrically refrigerated chamber. The refrigeration unit is capable of cooling to a temperature below -20°C. Bias for the tube is supplied by a Fluke Model 412 High Voltage Power Supply set at -1760 volts.

The output from the photomultiplier is fed to an SSR Instruments Co. Model 1120 Amplifier/Discriminator whose output is an input to a Model 1108 Multi-Mode Processor Photon Counter. The counting system is adjustable; its count time ranges from one microsecond to 1000 seconds, with a pulse pair resolution of 12 nanoseconds, and a maximum signal rate of 85 MHz. The counting time for the experiment is one second. The photon counter has a digital readout display. Next the digital signal is converted to an analog signal and amplified by a log-amplifier. Finally, the log signal is plotted by an xy plotter Model 560 supplied by Honeywell. The scanning speed is 0.05cm/sec.

For detection of gallium, light gathered by the 3½ inch diameter convex quartz lens is chopped by a PAR Model 191 variable speed chopper. The spectrometer is a Spex Industries Model 1799-II 3/4 meter Czerby-Turner spectrometer equipped with a Bausch and Lomb diffraction grating. The diffraction grating is 1000 lines/mm ruled and 3000Å⁰ blazed. The spectrometer is set at 4172.0Å⁰ which is the wavelength of light emitted by gallium. The entrance and exit slit widths are set like those on the other spectrometer. The output at the spectrometer exit slit is detected with a Spex Model 1424 photomultiplier. The photomultiplier output is fed to PAR Model 221 and 116 pre-amplifiers and then to a PAR Model 124A Lock-In Amplifier. The lock-in amplifier is capable of accurate signal measurements from 0.2 Hz to 210 kHz. The

output of this amplifier is recorded on the y-axis of a Fouston Instrument Omnigraphic 300 xy Recorder. The y-axis sensitivity ranges from 1 to 2000 millivolts/inch. The x axis represents sputtering time and it moves with speeds ranging from 0.5 to 20 inches/min. The speed is set at 1 inch per min. for this experiment.

VI Illumination of the Entrance Slit

Principle of Slit Illumination

The fundamental quantity in determining the illumination of the spectra, in most applications of the spectrograph, is the flux of energy per unit solid angle through the instrument (Ref 13:37). In GDOS, a spectrometer is used instead of a spectrograph; therefore, higher illumination of the spectra corresponds to higher sensitivity of the GDOS, i.e. stronger output.

The collimator mirror subtends at the slit a solid angle. Of the light which enters through the slit, only the part that is conformed in this solid angle is useful. The other part does not fall on the mirror and is wasted (Ref 13:37).

A case for an object with a surface of uniform brightness was analyzed in reference 13. All the light which enters through the slit within the solid angle bounded by planes V, V', H, and H' falls onto the collimator (See Figure 14).

If the light source is not large enough to produce the maximum condition described above, condensing lenses may be used to increase the sensitivity. This is the situation in the existing GDOS. The proposed steps to increase the sensitivity are to rotate the spectrometer by 90 degrees so that the edge of the cathode glow region may be imaged along the

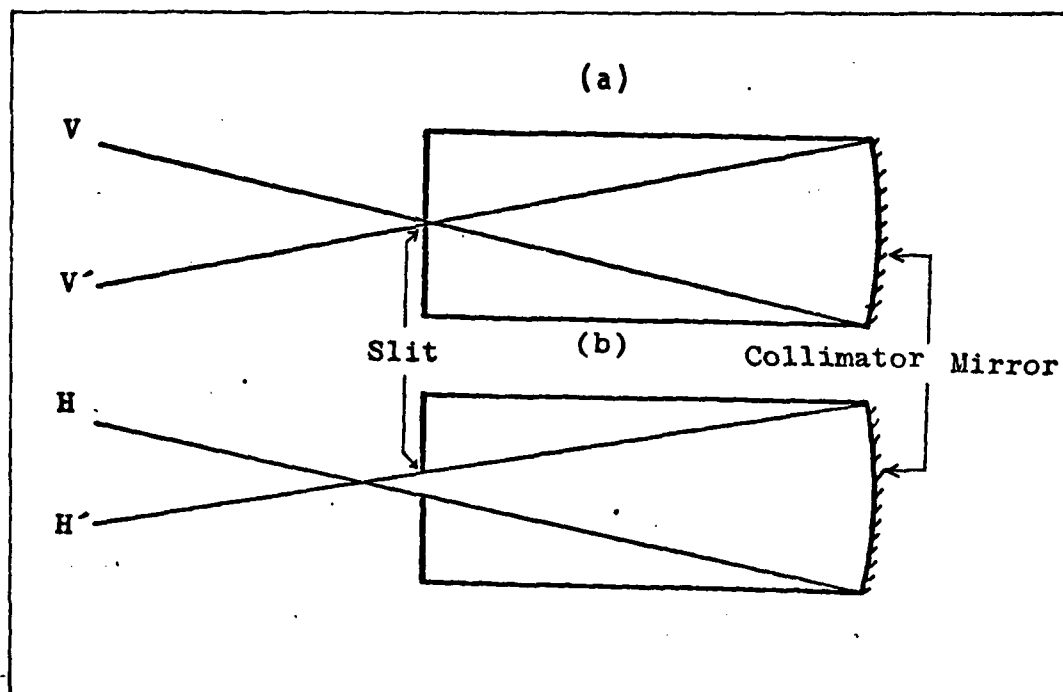


Figure 14. Illumination of the Collimator Mirror through a Rectangular Slit. (a) top views (b) side view (Ref 13).

slit height and to design a new optical input system. The optical system includes two lenses (See Figure 15). One is a cylindrical lens (L_1) of length equal to the diameter of a quartz window and focal length one centimeter longer than the distance between the center of the cathode and the window. The lens is horizontally placed such that the optical axis, OO' , bisects its length; it is also placed such that its focal point falls on the cathode center.

According to basic geometric optics, paraxial rays from the focal point are parallel to each other and to the optical axis after refraction whereas those from other points on

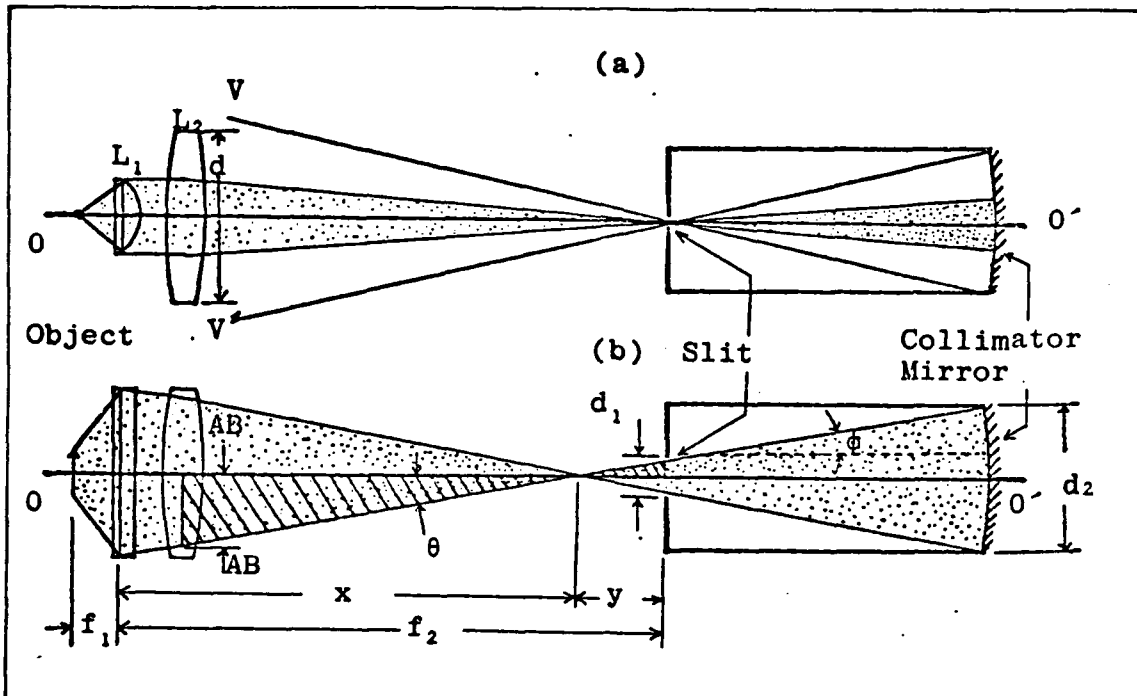


Figure 15. Optical Input System for GDOS. (a) Side View, (b) Top View

the focal plane are also parallel to each other, but not to the axis. The second lens (L_2) is a convex lens with diameter equal to the length of the first one. It is placed directly after the first one. All parallel rays converge to form a real image at its focal point.

The problem is to determine the focal length, f_2 , of the second lens such that the system gives the maximum illumination condition. Three assumptions are made for the calculation. The object, as viewed edge-on from the slit, is assumed to be just a straight line, i.e. the width is neglected. It is also assumed that the object is uniformly bright over the length. The third assumption is that AB is approximately

equal to half a diameter of the convex lens. From Figure 13b, the focal length of the convex lens is the sum of x and y .

$$f_2 = x+y \quad (27)$$

The distance x and y can be calculated by a simple trigonometric relation when θ is known.

$$x = (d/2)\cot\theta \quad (28)$$

where

d = diameter of the convex lens

and

$$y = (d_1/2)\cot\theta \quad (29)$$

where

d_1 = slit height

The angle θ is equal to ϕ which is determined by the structure of the spectrometer.

$$\theta = \phi = \arctan(d_2 - d_1)/2l \quad (30)$$

where

d_2 = diameter of the collimator mirror

l = the distance from the slit to the mirror.

Design of the Optical Input System

For the spectrometer used in this experiment, the design parameters are given as the following:

$$d = 6.99 \text{ cm}$$

$$d_1 = 2.0 \text{ cm}$$

$$d_2 = 10.0 \text{ cm}$$

$$l = 109.22 \text{ cm}$$

From equation (30),

$$\begin{aligned} \theta &= \arctan(10.0-2.0)/2 \times 109.22 \\ &= 2.10^\circ \end{aligned}$$

And from equation(28)and(29), x and y are,

$$\begin{aligned} x &= (6.99/2)\cot 2.10^\circ \\ &= 95.43\text{cm} \\ y &= (2.0/2)\cot 2.10^\circ \\ &= 27.23\text{cm} \end{aligned}$$

Therefore,

$$\begin{aligned} f_2 &= 95.43 + 27.23 \\ &= 122.66 \text{ cm} \\ &\approx 1.20 \text{ cm} \end{aligned}$$

A better approach is to use the actual width of the cathode fall region instead of the first assumption. Now the ray tracing does not satisfy the condition of maximum through-energy if the second lens, designed previously, is used. The new value of f_2 is determined such that it optimizes the energy through the spectrometer.

VII Encapsulants

Dielectric films deposited on the sample surface serve two purposes. One purpose is to delay the sputtering of the implanted sample until the sputtering process reaches equilibrium. The other is to act as barrier to impurity out-diffusion.

The Air Force Avionics Laboratory employs three techniques for film deposition. In the low pressure chemical vapor deposition (LPCVD), the gaseous sources are brought together in the reaction chamber and a chemical reaction is induced by heat at a typical temperature of 900°C. The plasma-enhanced chemical vapor deposition (PECVD) is actually a CVD process except that the chemical reaction is induced by a glow discharge plasma. Typical temperature in the PECVD is 300°C. The third method is glow discharge sputtering film deposition in which a solid source is used as the cathode.

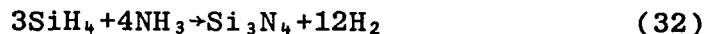
The LPCVD process is well established and widely used in industry. PECVD has been newly developed and just recently became available as a commercial production system (Ref 14). The glow discharge sputtering film deposition yields less consistent results which is presumably one of the reasons it has not found wide spread use in the industry (Ref 15).

For silicon nitride films, the common reactant gases in LPCVD and PECVD processes are silane (SiH_4) plus either

ammonia (NH₃) or nitrogen (N₂) or both. The chemical reactions are,



or



The silicon-implanted samples were encapsulated with aluminum nitride films instead of the commonly used silicon nitride film which could not be used due to the silicon content which would confuse the GDOS detection of implanted silicon. The films were deposited by the glow discharge sputtering technique.

According to reference 3, it appeared that the plasma-deposited film, from PECVD, was superior to the film deposited by LPCVD in the case of the annealed magnesium implanted samples. The superiority lay in that it minimized the out-diffusion of the impurities. However, studies have shown that the plasma-deposited film is only comparable to, not better than, the film deposited by the LPCVD process film (Ref 14). The only noticeable advantage of the plasma-deposited film is that it is deposited under low temperature which makes the process suitable for the passivation of temperature-sensitive devices.

VIII Experimental Procedure

Sample Preparation

All samples to be silicon implanted were cut from a group of wafers designated LDA1006 which are bulk grown, undoped, $\langle 100 \rangle$ oriented gallium arsenide.

The wafers were initially cut into rectangular pieces of $1 \times 0.5 \text{ cm}$ for handling convenience in the implantation process. The pieces were later cut into two $0.5 \times 0.5 \text{ cm}$ samples. The samples were cleaned with Aquasol (a mixture of soap and water); further cleaning was done with trichlorethylene, ethanol, and methanol consecutively in an ultrasonic shaker. The samples were etched in an etching solution before implantation to remove oxide. The solution was prepared from deionized water, hydrogen peroxide (H_2O_2), and sulfuric acid (H_2SO_4) by volume of 1:1:3 milliliters.

Ion implantation was performed in the Air Force Avionics Laboratory, using a modified accelerator manufactured by Accelerators, Inc. of Austin, Texas. The accelerator has a maximum implant energy of 120keV. Implantations were done at room temperature. The targets were mounted at approximately 7° from the normal to eliminate channelling.

Silicon was implanted at an energy of 120keV with fluences of 5×10^{14} , 1×10^{15} , and 3×10^{15} ions/ cm^2 . Two samples were double implanted at energies of 60 and 120 keV with a fluence of

1×10^{15} ions/cm². Magnesium was implanted at an energy of 120keV with a fluence of 3×10^{15} ions/cm².

Next, the samples were encapsulated and annealed. Cleaning before encapsulation was done by etching the samples in hydrochloric acid for one minute.

The magnesium implanted samples were encapsulated using a modified LPCVD reactor Model PND301 supplied by LFE Process Control Division, Waltham Mass. The reactant gases were silane and nitrogen; flow rates of the gases were 57.20 and 22.0 standard cubic centimeters per minute (SCCM) respectively. The RF power was 50 watts at a frequency of 13.56 MHz. The reaction chamber is a quartz bell jar vertically positioned. The chamber was evacuated to 5×10^{-2} μ Hg; and the pressure during deposition was 0.5×10^{-3} μ Hg. The substrate temperature was 220°C. Thickness and refraction index of the film were approximately 1000⁰Å and 2.0 respectively as measured with an ellipsometer supplied by Gaertner Science Corp. Chicago.

The silicon implanted samples were encapsulated with an aluminum nitride film. The sputtering system is a Model 2400 supplied by Perkin-Elmer, Randex. The aluminum nitride target was sputter cleaned for ten minutes in four and one microns of argon and nitrogen respectively. The RF power was 500 watts. The deposition lasted six minutes under the same conditions. The film thickness was approximately 500⁰Å.

Four silicon implanted samples with 1×10^{15} ions/cm²

were annealed at 900°C and four others with the same doses were annealed at 750°C. The annealing time was 20 minutes. All but two magnesium implanted samples were annealed at 900°C; times were 1,2,4,8,15, and 25 minutes.

Profiling Procedure

A step by step procedure goes as follows. Precautions must be taken to insure that the power supply to the photomultiplier tube is turned on only after the tube is fully cooled (approximately 15 minutes).

- a. Evacuate the sputtering chamber to 5×10^{-5} μmHg using rough, back and diffusion pumping sequence.
- b. Turn on the leak valve and let the pressure increase to 30 μmHg .
- c. Turn on negative high voltage, set at 3300V, for 1 minute.

This completes the so-called sputter cleaning.

- d. Turn off the vacuum pump.
- e. Open the leak valve, and load a sample in the chamber.
- f. Evacuate the chamber (approximately 1-2 hours) to 3×10^{-5} μmHg .
- g. Repeat b for 20 μmHg .
- h. Turn on the autotransformer (approximately 15 min.).
- i. Turn on the photon counter.
- j. Repeat c, with the voltage set at 2200V, and

immediately turn on both chart recorders.

- k. Let the system run until the impurity profile is completely recorded.

IX Results

Results from Silicon Implanted Samples

Measuring of silicon profiles was not successful. The GDOS failed to detect any silicon content in the implanted samples. Causes of this failure were suspected to be either the sensitivity or the absence of silicon itself or both.

The question of sensitivity was eliminated. This was done by using GDOS to detect and determine silicon concentration in a silicon bulk doped gallium arsenide wafer. A sample, 0.5x0.5cm, was sputtered under twelve different combinations of pressure and voltage from which one optimal sputtering condition was to be chosen. Consequently, a pure silicon sample was sputtered under those conditions to determine the proportionality constant for each case. The sputtering rate of the bulk-doped sample was $4340 \frac{\text{\AA}}{\text{min}}$. The results are tabulated in table III. It was evident that the number of counts increased with both pressure and voltage. The average silicon concentration was $6.28 \times 10^{19} \text{ atoms/cm}^3$.

The chosen sputtering condition was 15 μmHg and 3300V. One silicon implanted sample was profiled under these conditions, but there was still no evidence of a silicon profile.

Finally, two samples with $3 \times 10^{15} \text{ ions/cm}^2$ dose were analyzed by Secondary Ion Mass Spectroscopy (SIMS). The analysis was performed by Charles Evans and Associates, specialists

Table III

Results from Determination of Silicon Concentration
in a Bulk Doped-GaAs Sample.

Pressure μmHg	Applied Voltage kV	No. of Photon Counts		Si Concentration $\times 10^{19} \text{ atoms/cm}^3$
		Pure Si Sample	Si Bulk-Doped GaAs	
14	3.7	203,000	1,100	8.29
	3.5	182,000	700	5.84
	3.2	130,000	400	4.76
	3.0	102,000	330	4.98
15	3.5	204,000	900	6.76
	3.3	170,000	750	6.76
	2.5	55,000	165	4.61
	2.2	32,500	100	4.61
18	3.0	182,000	780	6.59
	2.8	142,000	650	7.04
	2.5	90,000	300	5.07
10	3.8	83,000	540	9.99

in materials characterization.

The conclusions were that no more than about 1×10^{14} ions/ cm^2 was present of $^{28}\text{Si}^+$; other species implanted were $^{28}\text{N}_2^+$ and $^{12}\text{C}^{16}\text{O}^+$, i.e. those with molecular weights of 28 amu. Figure 16 shows the relative magnitude of the profiles. Note that all profiles peaked at approximately the same depth and the silicon concentration is less than that of carbon and oxygen. This indicates that the cause of failure was due to the beam impurity during implantation.

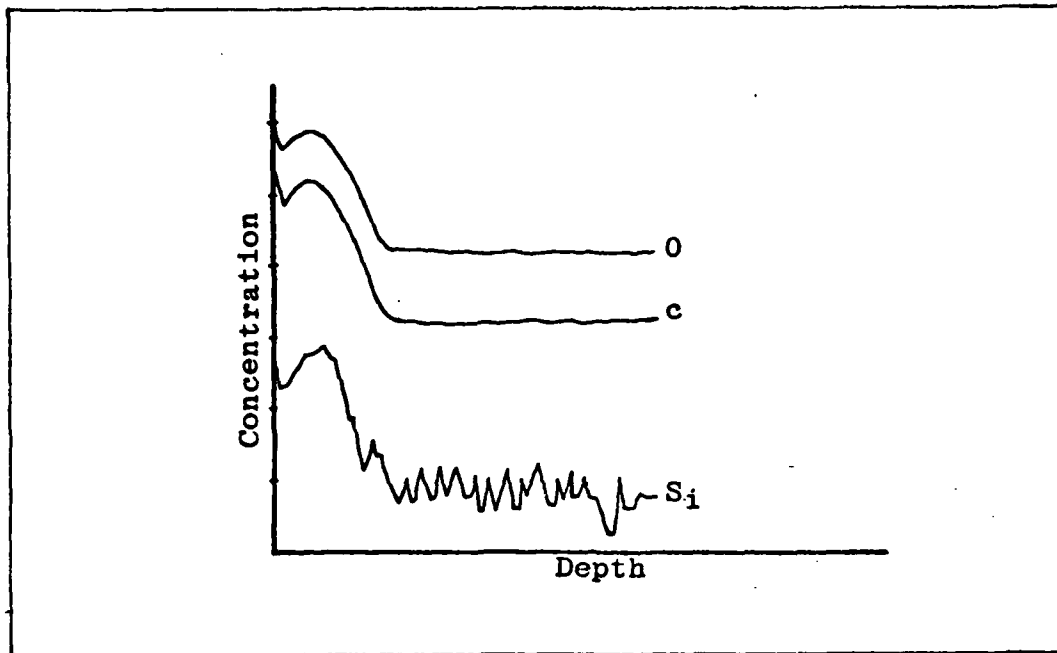


Figure 16. Sketched Profile Obtained from SIMS of Silicon Implanted Gallium Arsenide .

Results from Magnesium Implanted Samples

Typical output charts from GDOS are shown in Figure 17. The first step is to determine the location of the interface between the film and the substrate, which is to be referred to as zero depth. There is a step increase in photon counts in the gallium chart as the sputtering progresses through the interface. Ideally, it should be an abrupt step, but there is a small rise in time due to crossover diffusion. The rise times vary from sample to sample; the average is approximately 24 seconds. The zero depth lies somewhere in this interval; it is taken, for convenience, at the midpoint. Once

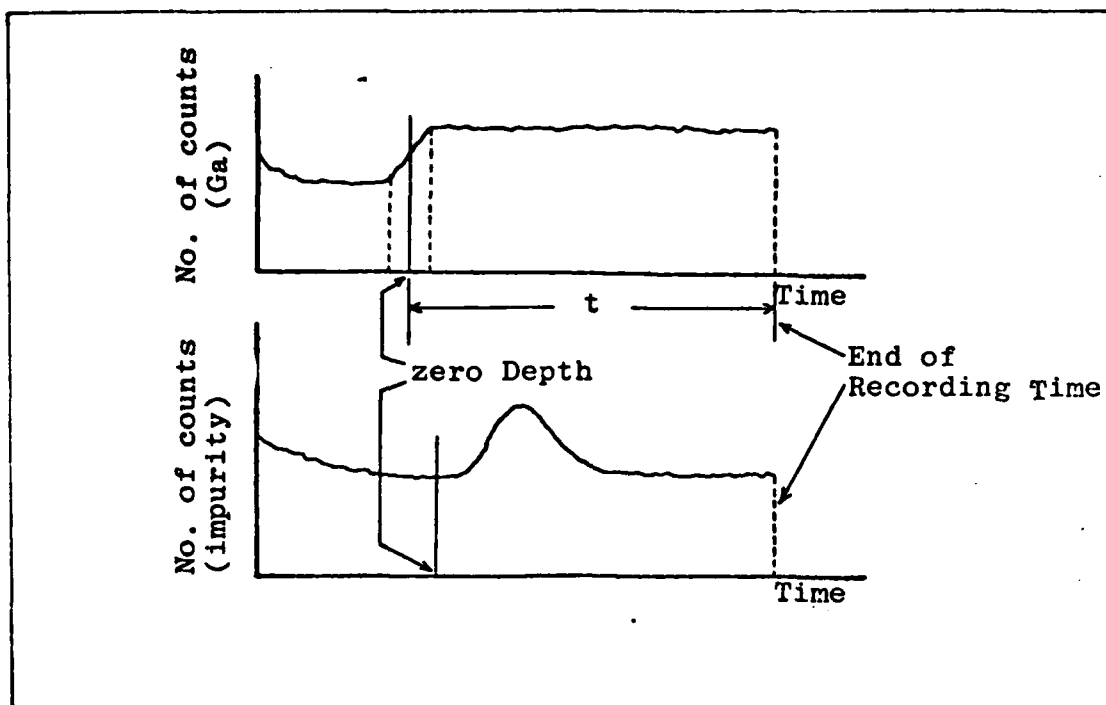


Figure 17. Typical Chart Outputs from GDOS

the zero depth is spotted, the time t from this point to the end of recording is determined. The sputtering distance from the zero depth to the end of recording point in the impurity chart equals the product of t and the scanning speed, 0.5cm/sec. Then the time axis is converted into a depth scale using the sputtering rate, 0.11 microns/min.

The theoretical prediction by the LSS theory of the magnesium implanted in gallium arsenide at energy of 120keV with fluence of 3×10^5 ions/cm² is given by equation (16),

where

$$\begin{aligned} \Delta R_p &= 0.05 \text{ } \mu\text{m} \\ &= 0.05 \times 10^{-4} \text{ cm} \end{aligned}$$

$$R_p = 0.12 \text{ } \mu\text{m}$$

$$N(x) = 2.4 \times 10^{20} \exp \frac{-(x-0.12)^2}{0.005}$$

$$N_p = 2.4 \times 10^{20} \text{ atoms/cm}^3$$

The measured profile of an unannealed sample is in close agreement with the order of magnitude of the predicted profile. The maximum concentration is smaller than the theoretical value by $1.2 \times 10^{20} \text{ atoms/cm}^3$. This may have been due to error in the assumed sputtering rate. If N_p were to agree with the theoretical value, equation (25) requires the sputtering rate of pure magnesium in this experiment to be 0.21 micron/min.

The peak is at a depth of 0.133 micron which is 0.013 micron deeper than the predicted value. The maximum error in the zero depth determination due to the rise time is 0.044 μm . The difference could have been due to inaccuracy of the zero depth determination.

All profiles of the annealed samples have one common characteristic. The overall profiles are shifted toward the region of radiation damage at the surface. Magnesium atoms also diffused across the interface into the silicon nitride films. The out-diffusion is so strong that all peak concentrations are in the film. The maximum and minimum peak concentrations are $4.69 \times 10^{21} \text{ atoms/cm}^3$ and $1.8 \times 10^{21} \text{ atoms/cm}^3$ respectively. The maximum and minimum distances from the peaks to the zero depth are 0.015 μm and 0.009 μm respectively. The

out-diffusion does not seem to be a linear function of annealing time. For example, it is intuitively expected that a peak should diffuse further out for a longer annealing time. This is certainly not true, if the determinations of the zero depths are accurate. For example the distance of the 25 minute annealing time is less than that of the one minute annealing time. The variation of N_p 's is a result of the relative ease with which magnesium diffuses through the films, which may have been caused by nonuniformity of the films themselves. The results are plotted in Figures 18 through Figure 23, and the maximum concentrations together with the distances are tabulated in Table IV.

It is clear that magnesium atoms have a very high diffusion coefficient in the radiation-damaged gallium arsenide. The diffusion is so fast that most atoms have already diffused out before any damage could be restored. It is also evident that the plasma-enhanced silicon nitride film is an excellent barrier to magnesium diffusion, in that the peak of the profile remains near the film-substrate interface.

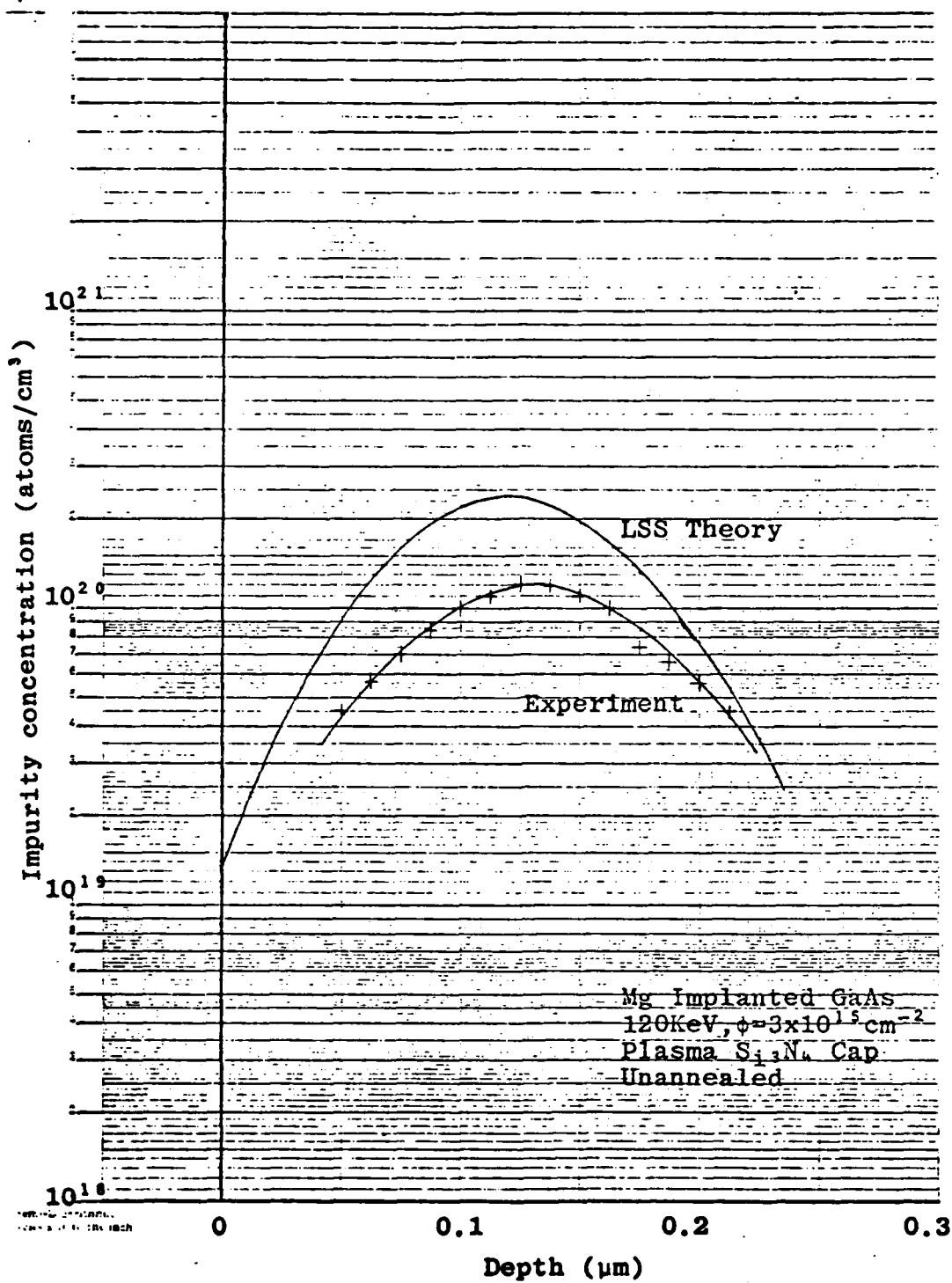


Figure 18. Measured Profile of Implanted Gallium Arsenide

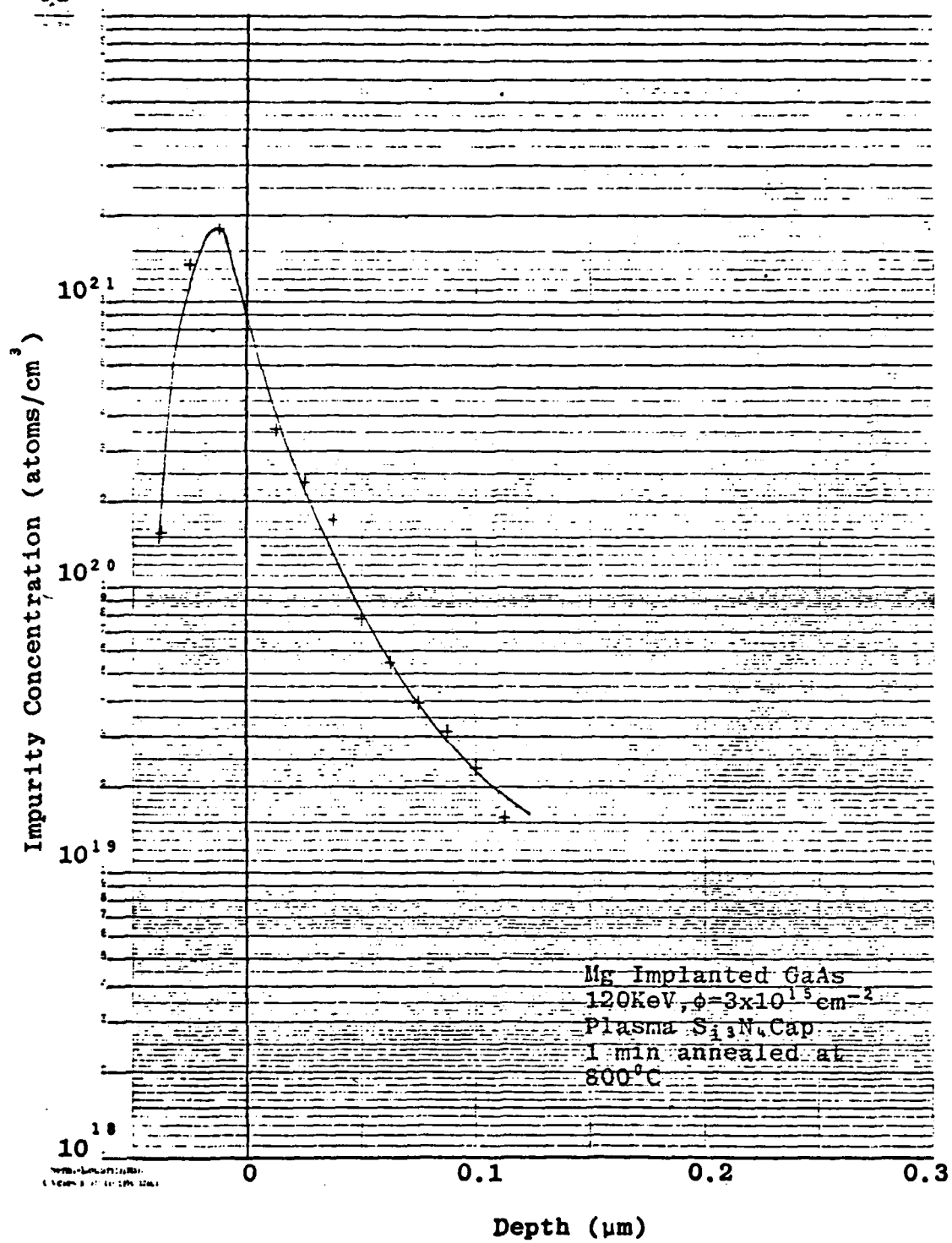


Figure 19. Measured Profile of Mg Implanted Gallium Arsenide

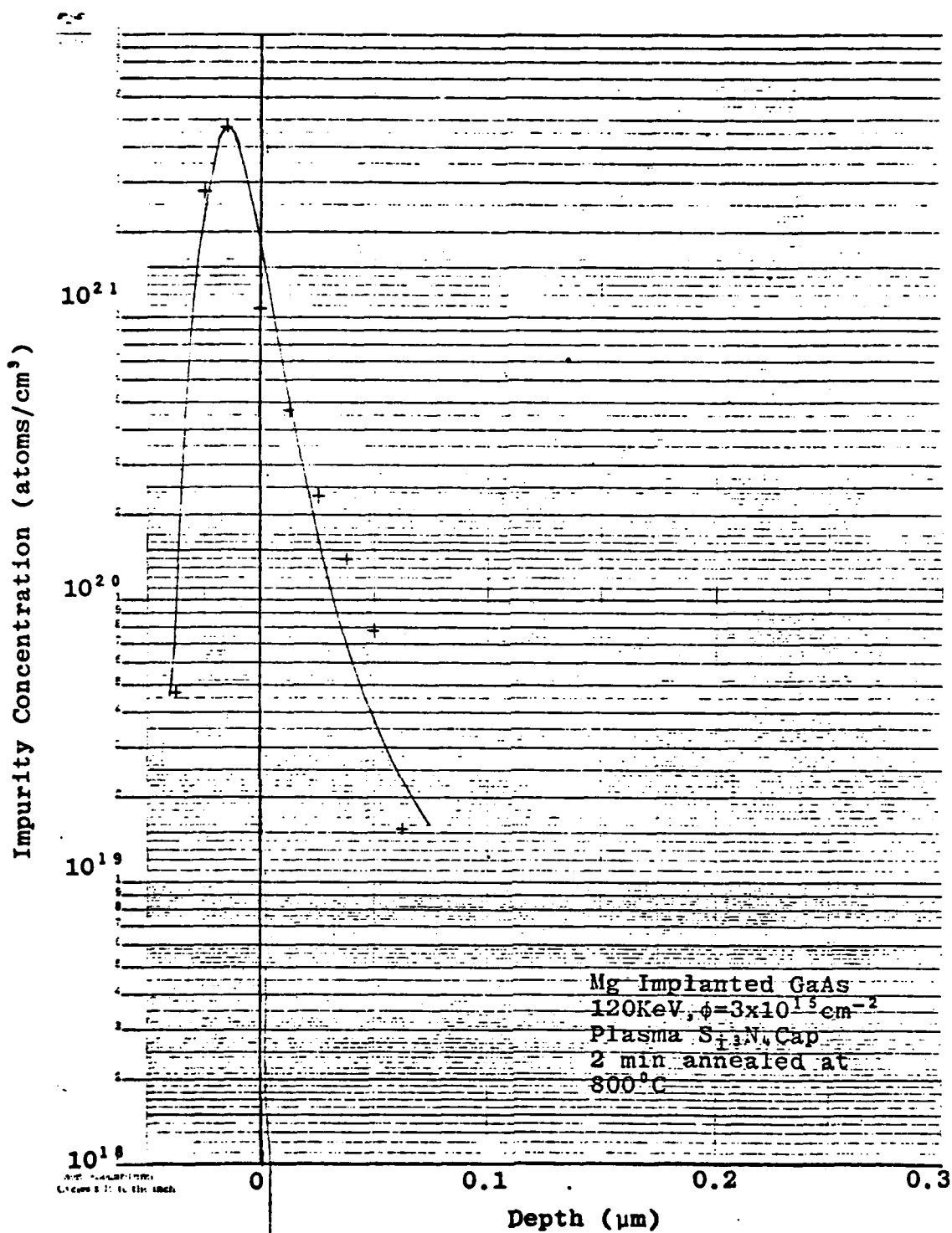


Figure 20. Measured Profile of Mg Implanted Gallium Arsenide.

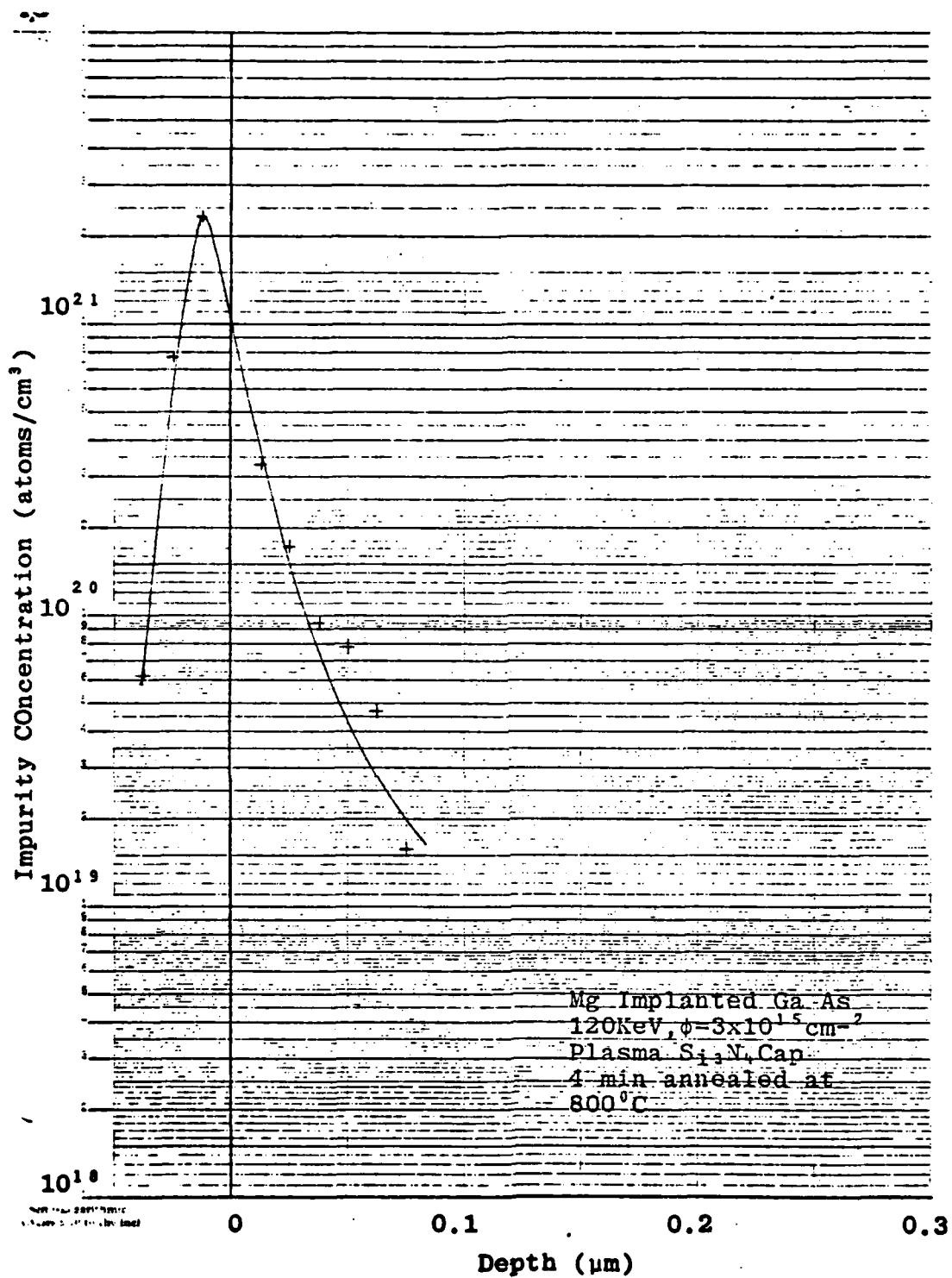


Figure 21. Measured Profile of Mg Implanted Gallium Arsenide.

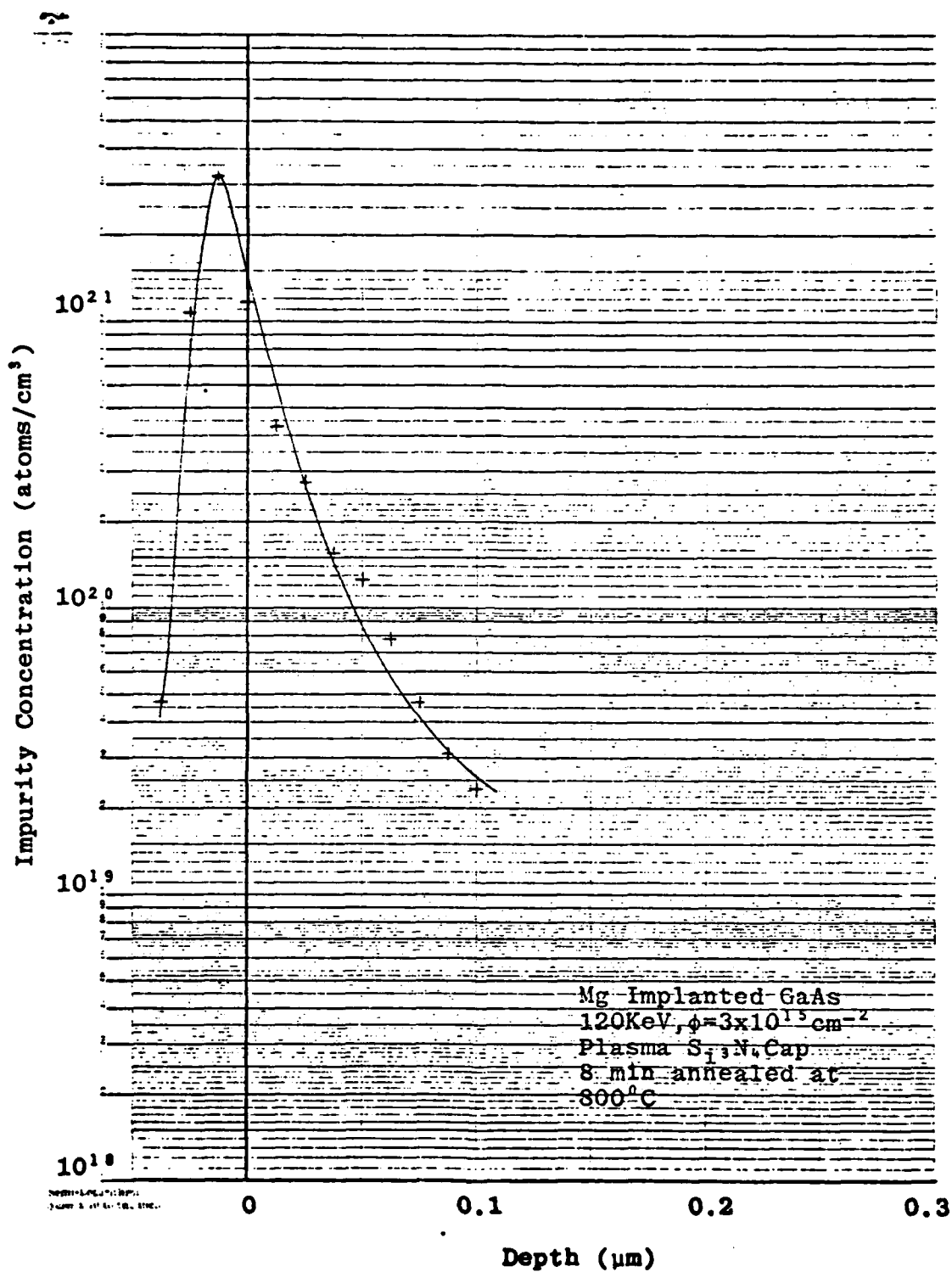


Figure 22. Measured Profile of Mg Implanted Gallium Arsenide

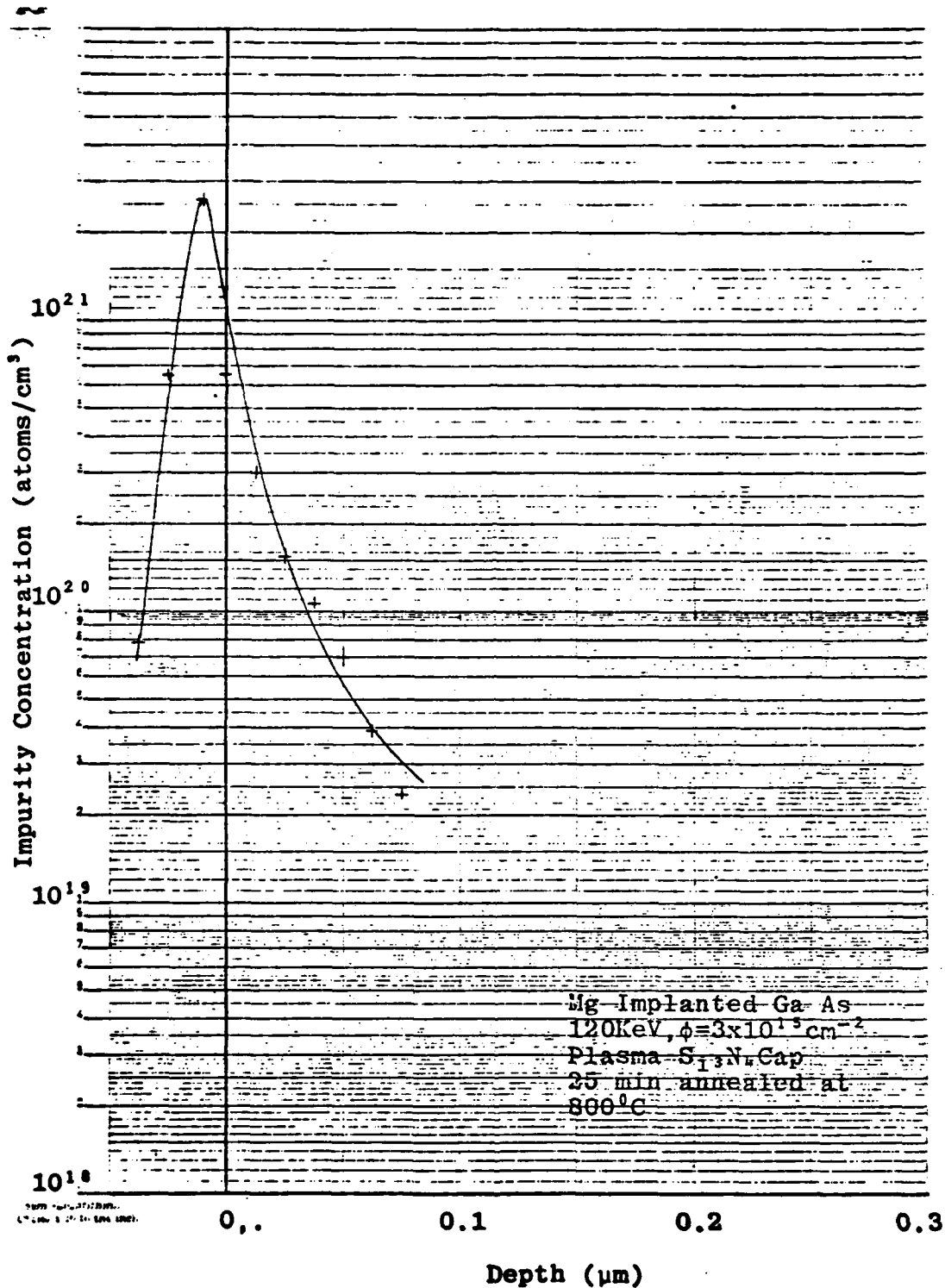


Figure 23. Measured Profile of Mg Implanted Gallium Arsenide

Table IV

Peak Concentrations and Distances into Si_3N_4 film
from 800°C Annealed Mg Implanted GaAs.

Anneal Time (Min)	Peak Concentration ($\times 10^{21}$ atoms/ cm^3)	Distance into the Film of Peak. (μm)
1	1.80	0.013
2	4.69	0.015
4	2.34	0.009
8	3.2	0.013
25	2.61	0.011

X Conclusion and Recommendations

Conclusion

The accuracy of impurity profiles measured by GDOS technique depends on the proportionality constant C and the zero depth determination. In the derivation of the proportionality constant C , it was assumed that k is constant in every measurement under the same sputtering conditions. It is then desirable that the sputtering rates of the calibration sample, B_s , be exactly equal to those of the samples, B_i , to be profiled. This is not always possible but the assumption on k is still valid as long as the ratio of B_s and B_i is close to unity.

The error on the zero depth determination causes the profile to shift from its actual location. The error can be minimized by selecting the film so that the cross-diffusion is minimum.

Magnesium impurity profiles were completely altered from what is predicted by the LSS theory. Magnesium atoms diffused toward the radiation damaged side of the samples. The impurity atoms also diffused into the silicon nitride encapsulants. The diffusion coefficient of magnesium in the samples was so large that the peak concentrations moved into the films for annealing times as short as one minute. Because annealing is necessary after ion implantation, the fast

diffusion eliminates one advantage of implantation of magnesium in gallium arsenide, that of putting the profiles completely beneath the substrate surface. If the final profiles after annealing which we actually obtained are desirable, then the implantation is still a useful doping technique. However, the surface concentrations are not easily predicted.

The physical properties of the plasma-deposited silicon nitride films are comparable to those of the films deposited by the CVD process. The only real advantage is that the film is deposited under a lower temperature which makes it suitable for the passivation of temperature sensitive devices.

Recommendations

1. Further work in the GDOS system should be directed to improving the sensitivity in order that the system may be used to analyze samples with low impurity concentrations. It is recommended that the spectrometer be rotated by 90 degrees and the design of the optical input system in section VI be implemented.

2. The output from the photon counter is a digital signal. In the present system, the output is converted to an analog signal, then it is log-amplified. Another alternative is to record the digital output directly. This requires an interface unit and a digital signal recording unit. Data can then be processed with a computer or a microprocessor.

Bibliography

1. Lindhard, J., M. Scharff, and H. Schiott. "Range Concept and Heavy Ion Ranges." Kongelig Danske Videnskabernes Selskab, Matematisk-Fysiske Meddelelser, 33:1-39(1963).
2. Williamson, K., "Glow Discharge Optical Spectroscopy of Ion Implanted Gallium Arsenide." Air Force Institute of Technology, WPAFB, Ohio: Thesis (December 1978).
3. Dearnaley, G. et al, Ion Implantation, New York: American Elsevier Publishing Co. Inc., 1973.
4. Gibbons, J.F. "Ion Implantation in Semiconductors-Part I: Range Distribution Theory and Experiments." IEEE Proceedings, 56:295-319 (March 1968).
5. Townsend, P.D., J. Kelly, and N. Hartly, Ion Implantation, Sputtering and Their Applications, New York: Academic Press Inc., 1976.
6. Brice, D., Ion Implantation Range and Energy Deposition Distributions. Vol I High Incident Ion Energies. New York: Plenum Press, 1975.
7. Smith, B., Ion Implantation Range Data for Silicon and Germanium Device Technologies, Oregon: Research Studies Press Inc., 1977.
8. Galaser, A., Integrated Circuits, Reading: Addison-Wesley Publishing Co., 1977.
9. Green, J., "Optical Spectroscopy for Diagnostics and Process Control during Glow Discharge Etching and Sputter Deposition." J. Vac. Sci. Technol., 15(5), (Sept/Oct 78).
10. Berry, R., Hall P., and Harris M., Thin Film Technology, New York Cincinnati Toronto London Melbourne: Van/Nostrand Reinhold Co., 1968.
11. Anderson, G.S., "Atom Ejection in Low-Energy Sputtering of Single Crystals of fcc Metals and of Ge and Si," Journal of Applied Physics, 33:2017-2025, (Mar 1962).
12. Cooper, C.B., R.G. Hart, and J.C. Riley, "Low-Energy Sputtering Yield of the (111) and (111) Faces of GaAs," Journal of Applied Physics, 44:5183-5184 (Nov 1973).

13. Sawyer, R., Experimental Spectroscopy, New York: Dover Publication, Inc. (1963)
14. Kerm, W., R. Rosler, "Advances in Deposition Process for Passivation Films," J.Vac.Sci.Technol. 14(5):1082-1097 (Sept./Oct 1977).
15. Pliskin, W. "Comparison of Properties of Dielectric Films Deposited by Various Methods, " J.Vac.Sci. Technol. 14(5): 1064-1076 (Sept/Oct 1977).
16. Rand, M., D. Wonsidler, "Optical Absorbtion as a Control Test for Plasma Silicon Nitride Deposition," J. Electrochem. Soc. 125(1):99-101(January 1978).
17. Werner, K., J. Vossen, Thin Film Processes, New York, San Francisco London: Academic Press (1978).
18. Sinha, A., et al, "MOS-LSI Passivation," J. Electrochem. Soc. 125(4):601-608(April 1978).
19. Papoulas, J.D., Electrical Phomina in Gases, New York: American Elseview Publishing Co. Inc., 1973.
20. Mayer, W., L. Eriksson, and J. Davies, Ion Implantation in Semiconductors, New York: Academic Press, 1970.
21. Amick, J., G. Schnable, and J. Vossen, "Deposition Techniques for Dielectric Films on Semiconductor Devices," J. Vac. Sci. Technol., 14(5):1053-1060(Sept./Oct.1977).

Appendix I

Plasma Deposition of Silicon Nitride Films

Plasma-deposited silicon nitride is used for final passivation of large scale integrated circuit (LSI) devices. The film provides scratch and particle protection during mounting and bonding operations because it is a hard, adherent dielectric (Ref 16). It is a good moisture and alkali barrier and it provides excellent step coverage up to over 10,000⁰Å steps (Ref 14).

Background

The deposition process is actually a chemical vapor deposition process (CVD). It is named the plasma-enhanced chemical vapor deposition process (PECVD) because it is aided by a radio frequency glow discharge. Glow discharge plasmas are usually created at pressures in the 0.01-1 torr range by the action of an electric field on contained gas molecules. This causes the breakdown of the gas molecules into a variety of very reactive species including electrons, ions and atoms and molecules in ground or excited states (Ref 14). The chemistry of deposition is extremely complex and detailed reaction kinetics are not understood, largely because such deposition reactions are difficult to probe diagnostically as opposed to processes taking place exclusively in the gas phase (Ref 17: 343).

One very important reason for using PECVD is that the substrate temperature can be kept low, typically at 300°C. A low temperature chemical reaction is a direct consequence of the plasma which is said to be in a non-equilibrium state. In such a state, the plasma exhibits an effective free electron temperature of tens of thousands of degrees Kelvin while the ambient temperature (that of free atoms, radicals, or molecules) will be only hundreds of degrees Kelvin (Ref 17:336).

PECVD Systems

A simple laboratory PECVD system is shown in Figure 18. The vacuum system includes a mechanical pump and a diffusion pump. The reactor is made of a quartz tube vertically installed. The RF power is inductively coupled by a coil around the tube from an RF power generator through an appropriate impedance matching network. The reactant gas sources, nitrogen and argon-diluted silane, are introduced into the reactor through tubes. The gas composition is determined by mass flow meters. Substrates are placed on top of the heater contained inside the reactor.

Effect of Reactor Design

Another alternative to the system described is to use capacitively coupled RF power through two metal plates also placed outside the reactor. These two designs both lead to a significant radial variation of field density and hence a large film thickness variation across a substrate (Ref 14).

A remedy is a design (Ref 17:348-351) shown in Figure 19. The reactant gas mixture enters upward through the rotating center shaft and flows radially outward between the two electrodes. Unreacted gases and reaction by-products are exhausted at the bottom of the reactor through a pumping system.

Film Properties and Deposition Rate

Film properties are subjected to many variables which may be interdependent: reactor geometry, electrode configuration and separation, power level and frequency, gas composition and flow rate, gas flow direction and flow pattern, pressure, substrate temperature and any added gas diluents (Ref 17:337). There have been many studies done on film properties; but because of the variation of PECVD systems and conditions of deposition, it is very difficult to compare data concerning the film properties.

Sinha, et al., (Ref 18) investigated in detail the deposition, etch rate of buffered hydrofluoric acid (BHF), refractive index, and Si/N composition as functions of the following parameters: flow, pressure, substrate temperature, and RF power. Kerm, et al., (Ref 14) studied films grown in a reactor with radial flow of gasses similar to the scheme discussed above. The thickness variation was found to be within three percent. The following table contains properties of the film grown from SiH_4 , NH_3 at 300°C .

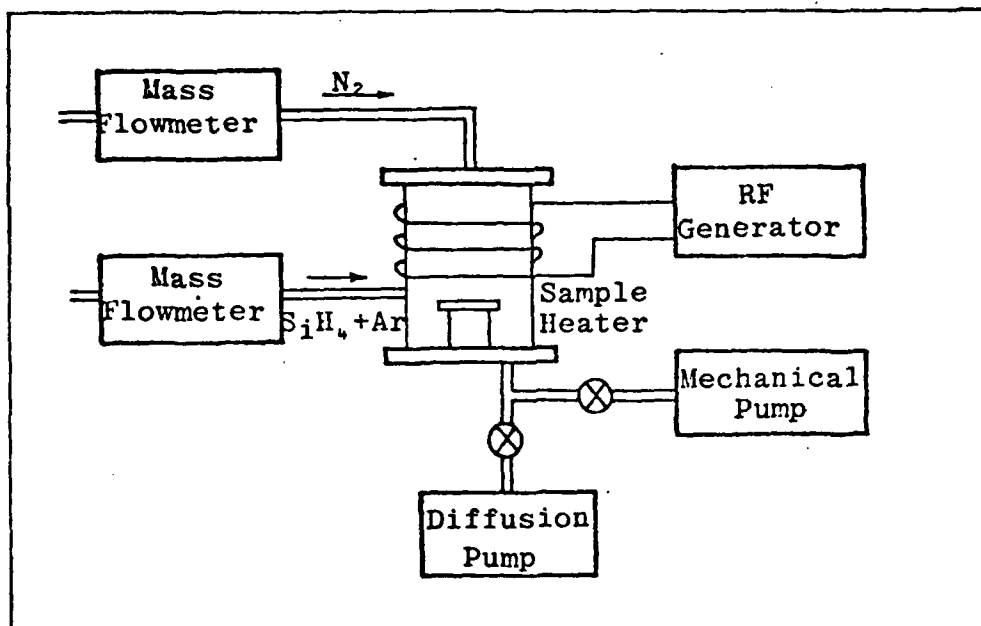


Figure 24. A Laboratory Plasma-Enhanced Chemical Vapor Deposition (PECVD) System (Ref 14:341).

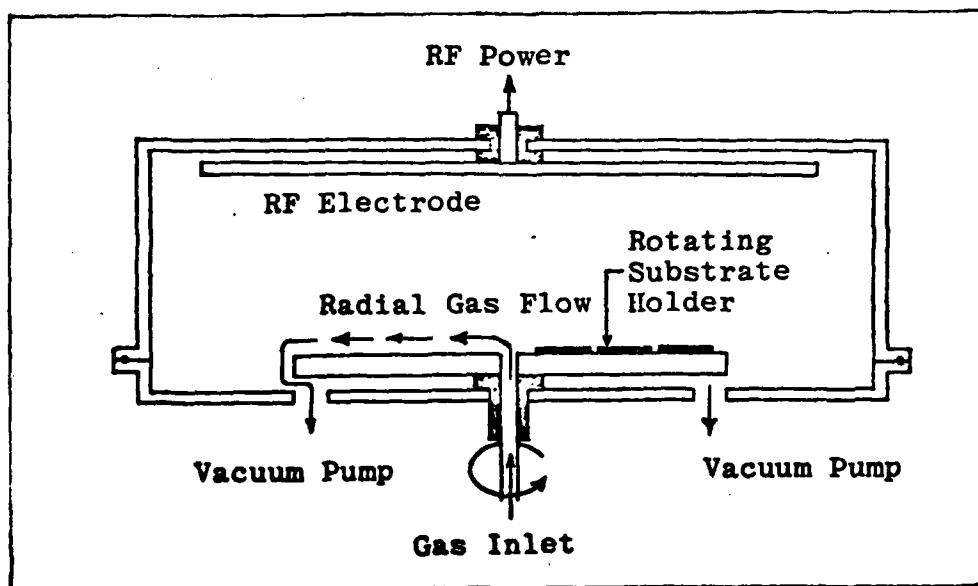


Figure 25. A Radial Flow Reactor Design (Ref 21).

Table V

Properties of Silicon Nitride Film from $\text{SiH}_4 + \text{NH}_3$ grown at 300°C

Density	2.5-2.8 g/cm ³
Refraction index	2.0-2.1
Dielectric constant	6×10^6 V/cm
Bulk resistivity	10^{15} Ωcm
Surface resistivity	1×10^{13} Ω/sq
Step coverage	conformal

VITA

Suk Puangthum was born on 17 July 1953 in Saraburi, Thailand. He graduated from Armed Force Academy Preparatory School in Bangkok in 1973 and entered Norwich University, in Northfield, Vermont, from which he received a Bachelor of Science degree with highest honors in May 1978. Upon graduation, he was commissioned in the Royal Thai Air Force. Immediately after graduation he entered the Air Force Institute of Technology, School of Engineering, in June 1978.

Permanent address:

39/1 Prayatod, Saohai

Suraburi, Thailand

UNCLASSIFIED

SECURITY CLASSIFICATION OF THIS PAGE (When Data Entered)

REPORT DOCUMENTATION PAGE		READ INSTRUCTIONS BEFORE COMPLETING FORM
1. REPORT NUMBER AFIT/GE/EE/79D-29	2. GOVT ACCESSION NO.	3. RECIPIENT'S CATALOG NUMBER
4. TITLE (and Subtitle) GLOW DISCHARGE OPTICAL SPECTROSCOPY OF ION IMPLANTED GALLIUM ARSENIDE		5. TYPE OF REPORT & PERIOD COVERED MS Thesis
		6. PERFORMING ORG. REPORT NUMBER
7. AUTHOR(s) Suk Phangthum		8. CONTRACT OR GRANT NUMBER(s)
9. PERFORMING ORGANIZATION NAME AND ADDRESS Air Force Institute of Technology AFIT/EN Wright Patterson AFB, Dayton, OH 45433		10. PROGRAM ELEMENT, PROJECT, TASK AREA & WORK UNIT NUMBERS
11. CONTROLLING OFFICE NAME AND ADDRESS Air Force Avionics Laboratory/DHR Wright-Patterson AFB OH 45433		12. REPORT DATE December 1979
		13. NUMBER OF PAGES 75
14. MONITORING AGENCY NAME & ADDRESS (if different from Controlling Office) AFAL/DHR Wright-Patterson AFB, OH 45433		15. SECURITY CLASS. (of this report) UNCLASSIFIED
		15a. DECLASSIFICATION/DOWNGRADING SCHEDULE
16. DISTRIBUTION STATEMENT (of this Report) Approved for public release; distribution unlimited		
17. DISTRIBUTION STATEMENT (of the abstract entered in Block 20, if different from Report)		
18. SUPPLEMENTARY NOTES Approved for public release; IAW AFR 190-17 JOSEPH P. HIPPS, Maj., USAF Director of Public Affairs		
19. KEY WORDS (Continue on reverse side if necessary and identify by block number) Glow Discharge Spectroscopy Plasma-enhanced Vapor Deposition Channelling in Single Crystal Materials Encapsulant Slit Illumination		
20. ABSTRACT (Continue on reverse side if necessary and identify by block number) An optical input system to an existing Glow Discharge Optical Spectroscopy (GDOS) apparatus was designed aiming to improve its sensitivity. The GDOS, unmodified, was used to obtain impurity concentration profiles of annealed and unannealed ion implanted gallium arsenide samples. Implant energy was 120 KeV. Silicon ions were implanted with fluences of 5×10^{14} ions/cm ² , 1×10^{15} ions/cm ² , and 5×10^{15} ions/cm ² . Magnesium ions were implanted with fluences of		

DD FORM 1473

EDITION OF 1 NOV 65 IS OBSOLETE

UNCLASSIFIED

SECURITY CLASSIFICATION OF THIS PAGE (When Data Entered)

UNCLASSIFIED

SECURITY CLASSIFICATION OF THIS PAGE(When Data Entered)

3X10¹⁵ ions/cm². Silicon implanted samples were encapsulated with aluminum nitride (AlN) films using a sputtering deposition technique. Magnesium implanted samples were encapsulated with 1000Å silicon nitride (Si₃N₄) films deposited by the plasma enhanced chemical vapor deposition (PECVD) method. Samples were sputtered in a low pressure argon filled quartz chamber. Light emitted from elements of interest was monitored. Light intensity was converted to impurity concentration by comparison to the light intensity emitted by a standard sample of the same element. A summary of PECVD technique is given in Appendix I.

UNCLASSIFIED

SECURITY CLASSIFICATION OF THIS PAGE(When Data Entered)